RESEARCH ARTICLE   **Open Access**

A study on benthic molluscs and stable isotopes from Kutch, western India reveals early Eocene hyperthermals and pronounced transgression during ETM2 and H2 events

Aniket Mitra, Rakhi Dutta* and Kalyan Halder

Abstract

The early Eocene greenhouse Earth experienced several transient global warming events, indicated by sharp negative excursions in the stable isotope ratios of carbon and oxygen. A huge amount of CO_2, enriched with ^{12}C, was released in the ocean–atmosphere system leading to warming. The Paleocene–Eocene boundary is demarcated by the most significant and well-known hyperthermal event, Paleocene–Eocene thermal maximum (PETM). The PETM is documented to be accompanied by a transgression. The later hyperthermals are relatively less studied. Information on the hyperthermals from the palaeo-tropical basins are relatively few. Here, we present a high-resolution litho-, bio- and isotope–stratigraphic analysis of the early Eocene succession from the Kutch Basin, western India. Stable isotopes of carbon and oxygen were analysed from sediments ($\delta^{13}C_{org}$) and mollusc shells ($\delta^{13}C_{carb}$ and $\delta^{18}O_{carb}$). The succession, prevailingly with lignite, along with carbonaceous black shale and plenty of fossil plant remains, is primarily a product of terrestrial environment. A pronounced marine transgression, characterised by marine mollusc bearing glauconitic shale in the middle of the succession, indicates a coastal transitional setting between the ocean and land. The $\delta^{13}C$ curve of organic carbon reveals five negative excursions, which are identified as the PETM, Eocene thermal maximum 2 (ETM2)/H1, H2, I1 and I2 in ascending order. The hyperthermal pair of ETM2–H2 corresponds with the marine interval. $\delta^{13}C_{carb}$ and $\delta^{18}O_{carb}$ from the middle part of the succession reveal concomitant negative excursions. The association between these hyperthermals and transgression appears to be regionally and globally valid, which strongly suggests a causal link between them.

Keywords: Early Eocene hyperthermals, Transgression, Fossil mollusc, $\delta^{13}C$, $\delta^{18}O$, Carbon isotope excursion, Kutch, Western India

Introduction

The late Paleocene–early Eocene time period had experienced several short-pulse hyperthermal events. A large amount of isotopically light carbon (^{12}C) was released in the ocean–atmosphere system, which is indicated by negative carbon isotope excursions (CIE) in the $\delta^{13}C$ curve of various proxies, such as bulk sediment organic carbon, bulk sediment carbonate, pedogenic carbonate and calcium carbonate remains of marine organisms. The Paleocene–Eocene thermal maximum (PETM) is the most well-known of these hyperthermals and widely reported from all over the world by a prominent excursion of the $\delta^{13}C$ curve of marine sedimentary and carbonate records at the Paleocene–Eocene (P–E) epoch boundary (~ 56 Ma) (Giusberti et al., 2007; Höntzsch et al., 2011; Sluijs et al., 2008, 2011; Stassen et al., 2012;

Westerhold et al., 2018; Zamagni et al., 2012). Coupled with the CIE, $\delta^{18}O$ from calcareous shells often showed a concomitant negative excursion. A negative excursion of $\delta^{18}O$ indicates an increase in temperature (Wright, 2001). A coupled negative excursion of $\delta^{18}O$ and $\delta^{13}C$ reflects an event of warming caused by the release of a large quantity of ^{13}C-depleted carbon in the ocean–atmosphere system.

The PETM was followed by several relatively smaller hyperthermal events during the early Eocene, which are ETM2 or H1 ($\sim$ 54.09 Ma), H2 ($\sim$ 54 Ma), I1 ($\sim$ 53.65 Ma), I2 ($\sim$ 53.55 Ma), J ($\sim$ 53.15 Ma) and ETM3 ($\sim$ 52.8 Ma) (Dickens et al., 1995, 1997; Lauretano et al., 2015; Westerhold et al., 2007, 2018). These hyperthermals are relatively poorly documented, especially from the tropical regions and terrestrial sites. Most of the known records are from relatively high latitudes and marine sequences.

A marine transgression has been recorded in association with the PETM from many parts of the world (e.g., Pujalte et al., 2014; Schulte et al., 2011; Sluijs et al., 2008, 2011, 2014; Speijer & Morsi, 2002). Although the transgression is generally considered linked to the PETM, there are records, where it has been observed to occur before the initiation of the CIE (Pujalte et al., 2014; Sluijs et al., 2008) posing questions as to their causal link. The onset of the transgression $\sim$ 20–200 Ky before the CIE associated with the PETM indicates that other factors were involved, such as a decrease of the sea basin capacity due to tectonism and volcanism (Sluijs et al., 2008). The proximal cause of the warming-induced transgression also remains equivocal. Thermal expansion of water and melting of Antarctic ice sheet as a response to the warming have been proposed to explain this transgression (Pujalte et al., 2014; Sluijs et al., 2008). The association of transgression with other hyperthermals is only tentative (Sluijs et al., 2008).

The Indian subcontinent was in the equatorial region during the early Eocene, following plate movement from the Southern Hemisphere to the Northern Hemisphere, after separation from the Gondwanaland in the Early Jurassic (Scotese, 2016; Smith et al., 1994). The Kutch Basin provides a sedimentary record from the Jurassic to Recent, punctuated by several stratigraphic breaks of different magnitudes. A significant break was associated with the emplacement of Deccan Traps during the Late Cretaceous. The Paleogene succession of the Kutch Basin rests upon the Deccan volcanics. Some other basins in the coastal areas of western India, such as Jaisalmer, Barmer and Bikaner of Rajasthan, and Cambay of Gujarat, record thick successions of the Paleogene rocks.

The early part of Paleogene sedimentary successions of most of the western Indian basins accommodates thick seams of lignite, which are being mined in open-cast mines. The recent geological investigations of these mine

sections yielded well-preserved fossils of vertebrates, and insects preserved in amber associated with the lignite seams (Bajpai et al., 2005; Folie et al., 2012; Kumar et al., 2007; Rana et al., 2013; Rose et al., 2009; Rust et al., 2010). Besides, time-diagnostic microfossils, foraminifers and palynomorphs, have also been reported from these mines (Agrawal et al., 2017; Garg et al., 2008; Paul et al., 2015; Rao et al., 2013; Singh, 2021). These fossils and a few isotopic analyses unambiguously indicate a Ypresian (early Eocene) age of the lignitic succession found from most of these mines (e.g., Khozyem et al., 2021; Punekar & Saraswati, 2010; Samanta et al., 2013). The middle part of the lignite bearing succession of these mines are characterised by marine mollusc rich layers, indicating a coastal marginal marine depositional setting. The marine interval, sandwiched between terrestrial lignite seams in these sections, indicates a transient transgression of the sea.

The first report of an early Eocene hyperthermal (EEH), i.e., ETM2, from India came from the Vastan mine of the Cambay Basin (Clementz et al., 2011). Later, Samanta et. al. (2013) reported five hyperthermal events, which are PETM, ETM2/H1, H2, I1 and I2, from two mines of the Cambay Basin, the Vastan and Valia mines. There are three mines, where active lignite mining is going on in the Kutch Basin near the localities of Panandhro, Umarsar and Matanomadh. The Panandhro and Umarsar, two large open-cast mines, are in the north-western part of the basin near Lakhpat Fort. The first report of an EEH from Kutch, which was tentatively identified as the ETM2, was from an outcrop section of the Ypresian succession (Khozyem et al., 2013). Later, the ETM2 was reported from the Panandhro mine, with a negative excursion of 2.7‰ (Agrawal et al., 2017). Recently, Khozyem et. al. (2021) reported the PETM and ETM2 from the same mine section. They have also reported these two EEH events from four other western Indian lignite mine sections (Khozyem et al., 2021).

The present study involves a detailed stratigraphic analysis of the lignite bearing succession from the Umarsar mine, Kutch, western India. The middle part of the succession includes marine mollusc bearing layers indicating marine incursion in this coastal basin. The sedimentological and palaeontological information are used to reconstruct the depositional environment. The study aims to find the early Eocene hyperthermals based on stable isotopic analyses of sediments ($\delta^{13}C_{org}$), and carbonates ($\delta^{13}C_{carb}$ and $\delta^{18}O_{carb}$) from fossil mollusc shells. Our analysis presents the record of the early Eocene high-resolution $\delta^{13}C_{org}$ data from the entire succession deposited in a transitional environment between the sea and land from a tropical setting. This is important in view of the very few available $\delta^{13}C$ records from tropical terrestrial sites for the early Eocene. We also present the $\delta^{13}C_{carb}$

and $\delta^{18}O_{carb}$ data from fossil mollusc shells from the middle part of the succession. Benthic and planktonic foraminifers have, so far, been predominantly used for such analyses. This is, as far as we are aware, the first report of $\delta^{13}C$ and $\delta^{18}O$ data from fossil molluscs from the Cenozoic. The present study also intends to investigate if the transgressive marine interval of the sequence is linked to any of the hyperthermal events. The study adds new data on the relationship of the ETM2 and H2 with the marine transgression during the early Eocene.

Geological setting

Kutch, a pericratonic rift basin in the western boundary of the Indian subcontinent, hosts a thick succession of the Mesozoic and Cenozoic sedimentary rocks, punctuated in the Late Cretaceous by the Deccan basalt. The basin was developed during the separation of the Indian subcontinent from the Gondwanaland in the Pliensbachian (Early Jurassic, 185 Ma) (Catuneanu & Dave, 2017; Scotese, 2016). It occupies a rifted graben in between the Nagar–Parkar uplift to the North, Radhanpur–Barmer arch to the East and Saurashtra uplift to the South (Biswas, 1992; Saraswati et al., 2018). The entire basin was flooded by marine incursion during the Middle Jurassic. The marine sedimentation continued in the Cretaceous before a fluvial system took over in the Late Cretaceous (Biswas, 2005). The Deccan Trap volcanics were emplaced over predominantly fluvial deposits of the Bhuj Formation. The sea began to inundate the basin again during the early Eocene. The regional slope of the basin is towards west–southwest (Catuneanu & Dave, 2017).

The Eocene succession of the Kutch Basin comprises the Naredi Formation, the Harudi Formation and the Fulra Limestone (Biswas, 1992). A fluvial flood–plain deposit, named the Matanomadh Formation of the Paleocene and characterised by clastics, volcanics, laterites and conglomerates, occurs below this primarily marine succession (Biswas, 1992). The Naredi and Harudi Formations are predominantly argillaceous with intercalations of carbonate and marl layers, and a few layers of silt and sandstone. Thin lenses of lignite occur locally in this argillaceous sequence. These two formations are separated by a phase of non-deposition and subaerial exposure, represented by a prominent laterite unit at the top of the Naredi Formation (Saraswati et al., 2016, 2018). The lower part of the Naredi Formation, the Gypseous Shale Member (Biswas, 1992), comprises alternations between shale beds of varied colours. Several levels containing mollusc fossils in this part and a foraminiferal limestone composed mostly of *Assilina* above it, the Assilina Limestone Member (Biswas, 1992), bear the signature of marine incursions in the middle of the Naredi Formation. An alternation of ferricretised siltstone/sandstone and bioturbated shale beds mark the upper part of the Naredi Formation—the Ferruginous Claystone Member (Biswas, 1992). The overlying Harudi Formation commences with an unfossiliferous shale unit with thin partings of silt. A 30 cm thick mollusc shell bed in the lower part and a meter-thick *Nummulites obtusus* bed in the upper part characterise the Harudi Formation (Biswas, 1992). The Fulra Limestone (Biswas, 1992), a carbonate platform deposition, is easily distinguishable from its underlying green–brown shale bed at the top of Harudi Formation, by its white-yellow colour and huge concentration of larger benthic foraminifers (LBF) dominated by the presence of *Nummulites* spp. and *Discocyclina* spp. (Banerjee et al., 2018). The age of the Naredi Formation is Ypresian (early Eocene), whereas that of the upper two formations is mostly Bartonian (middle Eocene) (Saraswati et al., 2016, 2018). The unfossiliferous upper part of the Naredi Formation and lower few meters of the Harudi Formation, including the mollusc shell bed, might include parts of the Lutetian (Banerjee et al., 2019; Halder & Das, 2019; Saraswati et al., 2016).

Mineable quantity of lignite occurs in the Eocene of Kutch. There are three active mines that exploit this lignite. The open-cast mine near the Panandhro village is well-studied, which yielded fossils of foraminifers, spore-pollen, dinoflagellate cysts and vertebrates (Agrawal et al., 2017; Bajpai & Theweissen, 2002; Khanolkar & Saraswati, 2019; Khozyem et al., 2021; Mathews et al., 2018; Sahay, 2011). The Umarsar mine lies about 5 km east of the Panandhro mine (Fig. 1). Having a similar lithologic succession, it is considered a lateral extension of the Panandhro mine (Shukla et al., 2019). Most recent studies support a Ypresian age of the lignite from the Panandhro mine (e.g., Agrawal et al., 2017). The palynomorphs found from the lower part of the Panandhro mine belong to the lower Eocene and have been reported from the lower Eocene rocks of Cambay, Kutch and Barmer basins of western India (Khozyem et al., 2021 and references therein). Some age-diagnostic palynomorphs, recovered from the upper part of this sequence, were known from the early Ypresian to early Lutetian from other parts of the world (Agrawal et al., 2017 and reference therein). Bajpai and Theweissen (2002) found a diverse assemblage of lower Eocene chordate fossils encompassing fish, turtle, snake and mammals from the Panandhro mine. All the lignite mine successions from Kutch and Cambay are characterised by a marine interval in the middle part. The presence of *Nummulites burdigalensis*, a LBF representing the Ypresian, in the marine part of these mines constrains the age of the marine unit to the early Eocene (Khozyem et al., 2021). This LBF is present in the Panandhro mine section (Khozyem et al.,
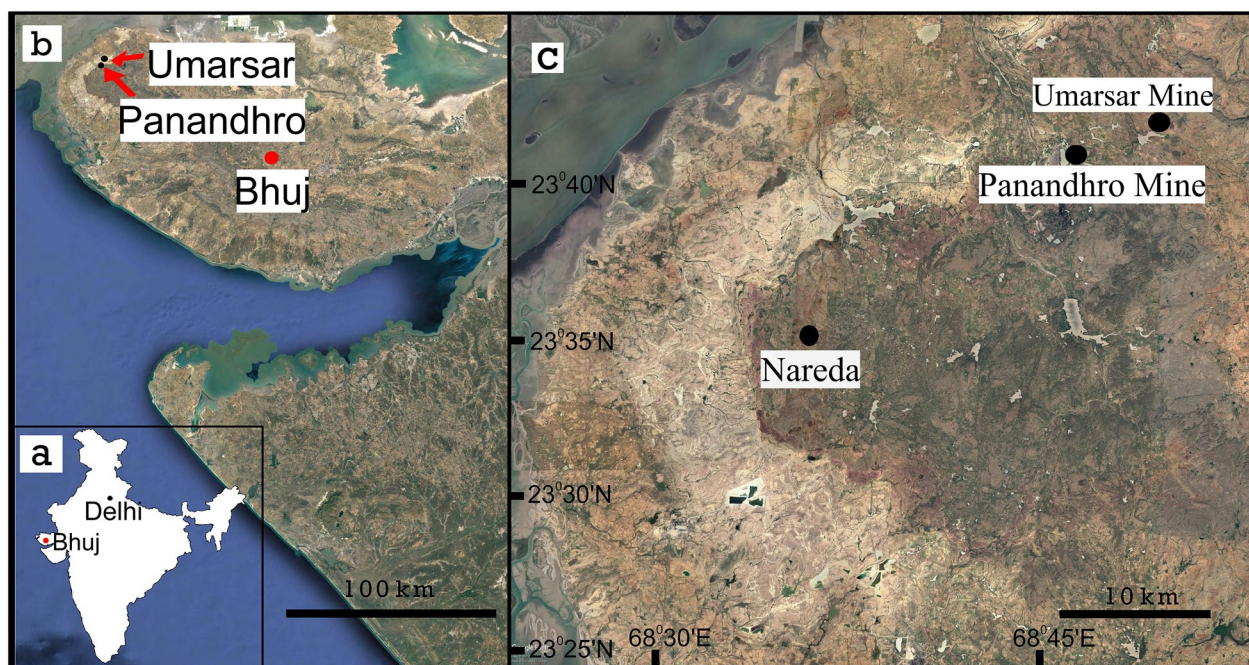
Fig. 1 Map of the study area in Kutch, India. **a** Map of India. **b** Position of the study area. **c** Location of the Umarsar and Panandhro mines. Nareda village, the type locality of the Naredi Formation is also shown

2021). Well-preserved marine molluscs are often present in the marine interval of these mines.

The lignites of Kutch were formed in a coastal swamp-marsh during a transgressive phase (Singh et al., 2017). Organic matters were derived predominantly from terrestrial or mixed terrestrial–marine settings (Khozyem et al., 2021; Sahay, 2011; Singh, 2021). The presence of rich coastal floral elements and diverse dinoflagellate cysts in the intervening layers of the lignitic sequence indicates a near shore environment (Mathews et al., 2018).

Materials and methods

The present study is primarily based on a drill core from the Umarsar mining area (23° 43′ 23″ N, 68° 50′ 03″ E) (Fig. 1). The mine sections were also studied. Samples have been collected from the drill core number 103 at an interval of 1 m. Sampling have been done at closer intervals, where lithology and/or fossil assemblage were found to change within 1 m.

Stratigraphy and fossils

The rock succession has been studied in detail to document the changes in lithological composition. The distribution of plant macrofossils, amber, pyrite and glauconite has been recorded. The stratigraphic distribution of mollusc fossils has been documented. The mollusc fossils

have been identified, wherever possible. We have interpreted their palaeoecological preferences based on the ecological affinities of their extant relatives and published literatures on fossil assemblages. The depositional environment and its changes through time have been interpreted using sedimentological and palaeontological information.

$\delta^{13}C_{org}$ and TOC measurement

Weighed samples of sedimentary rocks from the stratigraphic layers of the entire succession were acidified with 2 M hydrochloric acid and oven heated at 60 °C for 2 h and left for 24 h to allow all carbonate to be liberated as CO_2. The sample fractions were then isolated by centrifugation and the acid was decanted. The samples were then washed twice using distilled water and centrifugation.

The samples were analysed by the Elemental Analyzer–Isotope Ratio Mass Spectrometry (EA–IRMS) using Europa Scientific 20–20 IRMS. The reference material used during $\delta^{13}C_{org}$ analysis was IA R001 (wheat flour) having $\delta^{13}C_{VPDB}$ of $-26.43‰$. Further control materials analysed were IA R005 (beet sugar) and IA R006 (cane sugar) with $\delta^{13}C_{VPDB}$ of $-26.03‰$ and $-11.64‰$, respectively. These reference standards were calibrated against and traceable to IAEA-CH-6 (sucrose, $\delta^{13}C_{VPDB} = -10.43‰$). IAEA-CH-6 is an inter-laboratory comparison standard distributed by the International

Atomic Energy Agency (IAEA), Vienna. Both references and samples were prepared and analysed in the same manner. The analysis proceeded in a batch process, whereby a reference was analysed followed by a number of samples and then another reference. The analysis was repeated for 20% of the samples. The isotope analyses were carried out by ISO Analytical, UK.

X-ray diffraction (XRD) analysis

Fossil fragments of benthic mollusc shells were separated from weakly indurated clay layers of the drill core containing such fragments. Molluscan shell fragments were left overnight within a solution of hydrogen peroxide (H_2O_2) and de-ionised water in 3:7 ratio. The samples were then cleaned in an ultrasonic bath of de-ionised water and oven-dried at 50 ℃.

Powdered shell samples of three bivalve species, *Aphrodina* sp., *Caestocorbula* sp. and *Claibornicardia* sp., which are common in different levels, were used for the analysis. XRD analysis was performed in a Rigaku Smartlab high resolution X-ray diffractometer (HRXRD) machine at the central research facility of IIT-ISM Dhanbad, India. The HRXRD machine has 3 kilo-watt source and Cu Kα radiation, and is equipped with a high resolution HyPix-3000 semiconductor detector. The optimum scanning range in XRD is set between 5 and 60°. The data was then analysed by comparing d-spacings with the help of Profex 5.0.2 software (Doebelin & Kleeberg, 2015).

### $\delta^{13}C_{carb}$ and $\delta^{18}O_{carb}$ measurement

Mollusc shells with known aragonitic composition were used for this analysis. Weighed powdered samples of the shell fragments were flushed with 99.995% helium and then treated with phosphoric acid. The reaction with acid was allowed to take place overnight in room temperature. The CO_2 gas liberated from the samples was then analysed by Continuous Flow Isotope Ratio Mass Spectrometry (CF-IRMS) in Europa Scientific 20–20 IRMS. The reference material used during the analysis was IA-R022 (Calcium carbonate, $\delta^{13}C_{V\text{-}PDB} = -28.63$ ‰ and $\delta^{18}O_{V\text{-}PDB} = -22.69$‰). Other control samples used were NBS-18 (carbonatite, $\delta^{13}C_{V\text{-}PDB} = -5.01$‰ and $\delta^{18}O_{V\text{-}PDB} = -23.20$‰) and IA-R066 (chalk, $\delta^{13}C_{V\text{-}PDB} = +2.33$‰ and $\delta^{18}O_{V\text{-}PDB} = -1.52$‰). IA-R022 was calibrated against and traceable to NBS-18 and NBS-19 (limestone, $\delta^{13}C_{V\text{-}PDB} = +1.95$‰ and $\delta^{18}O_{V\text{-}PDB} = -2.2$‰). IA-R066 was calibrated against and traceable to NBS-18 and IAEA-CO-1 (carrara marble, $\delta^{13}C_{V\text{-}PDB} = +2.5$‰ and $\delta^{18}O_{V\text{-}PDB} = -2.4$‰). NBS-18, NBS-19 and IAEA-CO-1 are inter-laboratory comparison standard materials distributed by IAEA. Repeat measurements were done for 20% of the samples. The analysis was done by ISO-Analytical, UK.

Results

Lithostratigraphy and fossils

The studied section is a 94.5 m thick drill core of the Umarsar lignite mine. The lithology is dominantly argillaceous and composed of varied shale and mudstone beds (Fig. 2). The mine sections, as well as the drill core, do not exhibit any unconformity. The entire section records fossil plant remains including leaf impressions (Figs. 2, 3a). Amber, in nodular and small granular forms, is also found dispersed through the entire succession (Figs. 2, 3a, b). Here, the succession is informally divided into four litho-units (Fig. 2). The lowermost 10.5 m thick unit, unit 1, is dominated by mudstones, containing pyroclastics and sand laminae (Figs. 2, 3c). Very small amount of plant remains and amber are present in this basal unit. The overlying 41 m thick (from 89.5 to 49.5 m) succession, unit 2, accommodates mainly light grey shale with a 1-m thick unit of lignite at 66.5–65.5 m depth (Fig. 2). Black shale beds are common in the middle part of this grey shale unit. Two meters of brown shale with thin laminae of sandstone has been recorded at 74.5–76.5 m depth. This grey–black shale is rich in plant remains and amber (Figs. 2, 3d, e). Glauconite has been found rarely in this unit (Figs. 2, 3f). Pyrite, in small quantity, is present in several layers of this unit (Figs. 2, 3g). The unit 3, predominantly composed of green shale with fossils of marine molluscs belonging to bivalves and gastropods, is the next 22 m of the depositional sequence (Figs. 2, 3h–j, 4, 5). A 2-m thick lignite seam is present in this unit at 38.5–40.5 m depth (Fig. 2). Two thin mollusc shell beds (limestone) are present in the upper part of this unit (Figs. 2, 3k, 4, 5g). Pyrite is abundant at 33.5 m to 34.5 m depth (Fig. 3j). Amber and plant remains are scarce in this green shale unit except at the vicinity of the lignite seam and its bounding layers. The overlying unit 4 begins with a meter-thick lignite unit at 26.5 m depth (Fig. 2). The unit 4, the uppermost 21 m of the succession, is predominantly an alternation between lignite, black shale and grey shale beds (Figs. 2, 3m, n). A layer of ferricrete is present at the top of this unit (Figs. 2, 3o).

The green shale unit (unit 3) contains marine fossils of bivalves and gastropods. The bivalves in the drill core are commonly broken and disarticulated. However, several identifiable specimens—large fragments or entire shells—have been recovered. The shells do not exhibit any preferred orientation but are commonly parallel to the bedding plane. The lowest part of the unit 3 is characterised by the members of Pteriidae (*Pteria* sp.), Anomiidae (*Anomia* sp.), Nuculanidae (*Nuculana* sp.) and Corbulidae (*Caestocorbula* sp.) families (Figs. 4, 5a–f). Venerid (*Aphrodina* sp.) and carditid (*Claibornicardia* sp.) bivalves (Figs. 4, 5g–j), along with members of Corbulidae dominate the rest of the sequence.
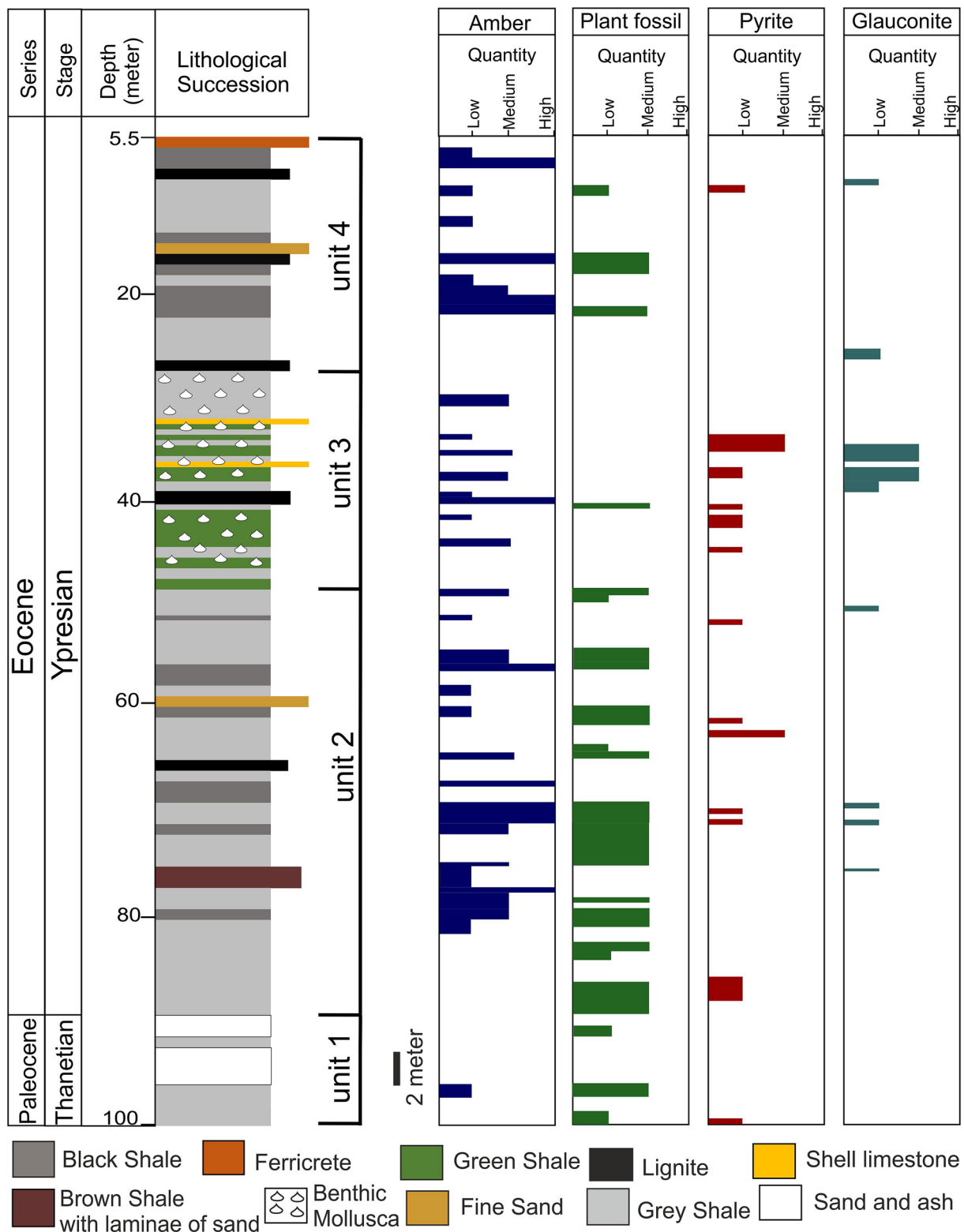
Fig. 2 Lithostratigraphic section of the Umarsar mine as revealed from the 103 no. drill-core. The four informal units of the succession are marked. Relative quantities of amber, plant matter, pyrite and glauconite in different levels are indicated

The proportion of *Claibornicardia* increases in younger parts, whereas *Aphrodina* is more common in the lower parts (Fig. 4). Members of the family Corbulidae are uniformly present throughout the unit 3 (Fig. 4). The shell beds are dominantly composed of *Claibornicardia*, *Aphrodina* and *Caestocorbula* (Figs. 3m, 4, 5g). Gastropods are mostly broken. However, based on a few identifiable specimens, the common gastropod fossils have been identified as belonging to the genus *Turritella* (Fig. 5k, l).

Total organic carbon
The content of TOC (%) varies from < 1 to ~ 50% (Fig. 6d, Additional file 1). The lignite units have highest level of TOC (> 35%). The TOC content varies between 10.28 and 35% in the carbonaceous black shale layers. The green shale layers record very low values (< 3%). The colour of grey shale darkens with increasing value of TOC, which ranges from ~ 1.8 to 12%. The shell limestone units also yielded very low values (0.27 to 0.88%) of TOC. The thinly laminated sandstone units have TOC of 0.28–3.19%.

Isotope stratigraphy
$\delta^{13}C_{org}$
The bulk sediment organic carbon $\delta^{13}C$ ($\delta^{13}C_{org}$) has been plotted against the lithostratigraphic column of the drill core no. 103 of the Umarsar mine (Fig. 6b). The mean $\delta^{13}C_{org}$ value of the entire sequence is -26.87‰ and the standard deviation is 0.56‰ (1σ, $n = 103$). The data set forms a bell-curve (Fig. 7). 69.90% (72 out of 103) of the data fall within the range of 1σ from the mean. The control samples wheat flour, beet sugar and cane sugar have shown a standard deviation of 0.07‰ (1σ, $n = 14$), 0.04‰ (1σ, $n = 10$) and 0.11‰ (1σ, $n = 10$), respectively. The repeat measurements of our samples exhibit an average deviation of 0.04‰ with maximum data falling between 0.02‰ (25 percentile) and 0.05‰ (75 percentile) (Additional file 1).

Five major negative excursions have been observed in the sequence (Fig. 6b). The first major negative CIE of 2.01‰ has been observed at 72.5 m depth in the studied section. This CIE occupies 20 m thick succession and comprises two pulses. The second CIE (= 2.12‰) occurs at 38.5 m depth and also consists of two pulses. The third CIE (= 1.25‰) is at 33 m depth and lies only 5.5 m above the second CIE. The fourth (= 1.83‰, at 24.5 m depth)

and fifth (= 1.38‰, at 20.5 m depth) CIEs are very close. A small negative excursion of 1.03‰ has been observed at 58.5 m depth lying between the first and second major CIEs.

XRD analysis
The diffraction angle (2θ) and X-ray intensity obtained from the analysis of three shell fragments are plotted (Fig. 8) and given in the Additional file 2. The peaks coincide with the standard d-spacings of aragonite, which are superposed on the plot (Fig. 8).
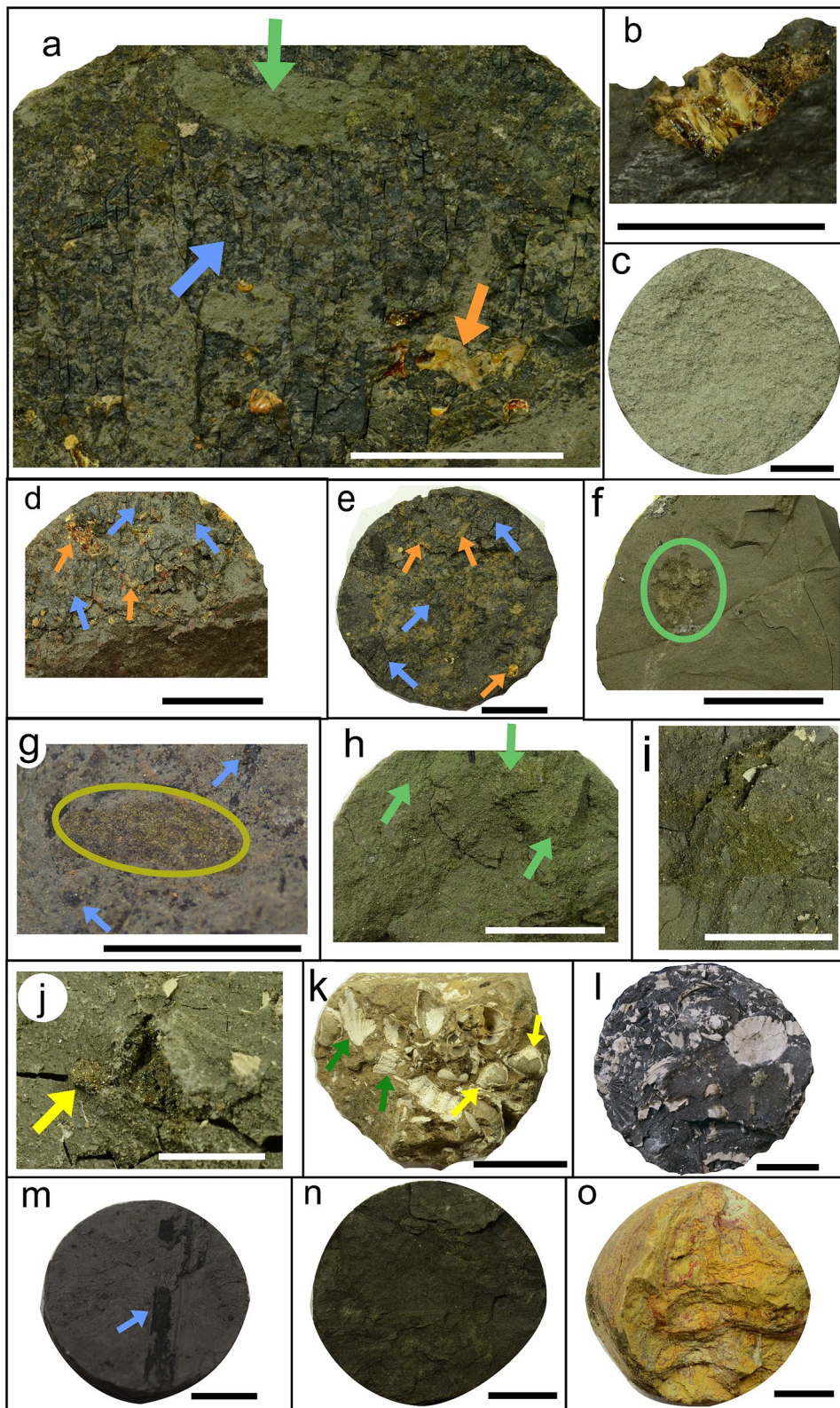
$\delta^{13}C_{carb}$ and $\delta^{18}O_{carb}$
The reference and control materials have shown standard deviations in the range of 0.01–0.02‰ for $\delta^{13}C_{carb}$ and 0.00–0.07‰ for $\delta^{18}O_{carb}$ (Additional file 1). Our samples also exhibit similar standard deviations in repeat measurements ranging from 0.00 to 0.06‰ for $\delta^{13}C_{carb}$ and 0.04 to 0.11‰ for $\delta^{18}O_{carb}$.
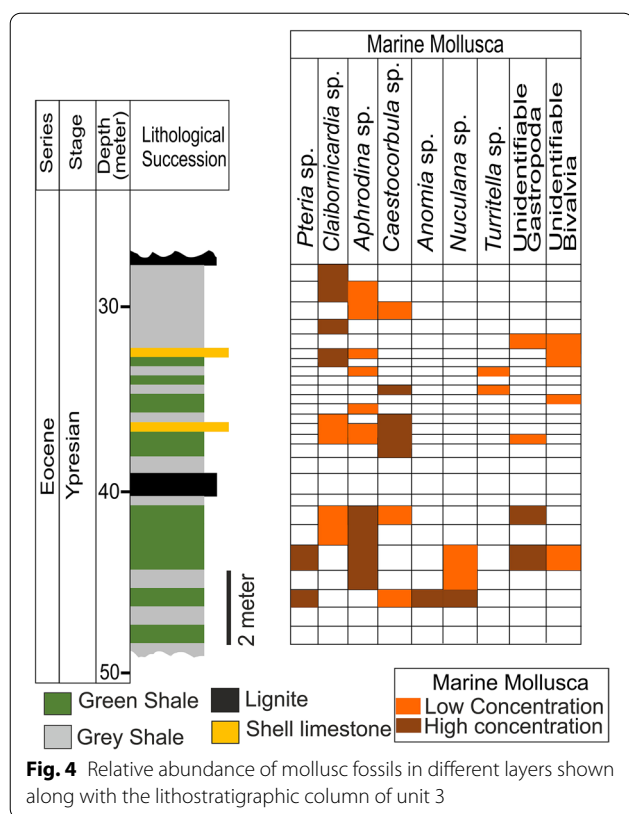
Fossil molluscs were found only from the unit 3 of the studied section. A few layers of this unit (lignite and adjacent grey shale) spanning about 4 m were barren. $\delta^{13}C_{carb}$ and $\delta^{18}O_{carb}$ data have been plotted against the litho-column of this part of the succession (Fig. 6c). The curves show concurrent negative excursions. The curves exhibit two pronounced negative excursions on either sides of the lignite seam (Fig. 6c). However, the values fluctuate rapidly in this part and there are slight mismatch in the details of peak positions in the two curves by 0.5 to 1 m. The first CIE below the lignite layer is -2.37‰. The value of the CIE above the lignite layer cannot be properly assessed because of the absence of data in this part. These two excursions mimic the two pulses of excursion in $\delta^{13}C_{org}$ associated with the ETM2, with slight difference in the position of the upper peak (Fig. 6b, c). The total excursion of $\delta^{13}C_{carb}$ is -2.5‰. The corresponding excursion in $\delta^{18}O_{carb}$ is -1.86‰.

There is a positive shift in the average value of $\delta^{13}C_{carb}$ in the upper part of the marine interval, which is not replicated by $\delta^{18}O_{carb}$ (Fig. 6c). However, the relative excursions in both the curves in this part, albeit short, conform to each other. An excursion of -0.80‰ in $\delta^{13}C_{carb}$ and -0.51‰ in $\delta^{18}O_{carb}$ match the CIE in $\delta^{13}C_{org}$ identified as H2 (Fig. 6b, c). Another shorter excursion between H2

(See figure on next page.)
Fig. 3 **a** Amber, plant fossil and glauconite pocket within shale indicated by yellow, blue and green arrows, respectively. **b** Granular amber within black shale. **c** Pyroclastics of unit 1. **d** Grey shale with amber (yellow arrow) and plant fossils (blue arrow) in unit 2. **e** Black shale with amber (yellow arrow) and plant fossils (blue arrow) in unit 2. **f** Grey shale with glauconite pocket (green oval) in unit 2. **g** Grey shale with pyrite (yellow oval) and plant matter (blue arrow) in unit 2. **h** Green shale in unit 3, glauconite indicated by green arrow; white dots are fragments of fossil molluscs. **i** Grey shale with pockets of glauconite and mollusc fragments in unit 3. **j** Green shale with pyrite (yellow arrow) in unit 3. **k** Shell limestone with mollusc fossils in unit 3; yellow and green arrows indicate *Caestocorbula* sp. and *Claibornicardia* sp., respectively. **l** Mollusc concentration in upper part of unit 3. **m** Black shale with plant fossil (blue arrow) in unit 4. **n** Lignite in unit 4. **o** Ferricrete in unit 4. Scale bars 10 mm

Fig. 3 (See legend on previous page.)

Fig. 4 Relative abundance of mollusc fossils in different layers shown along with the lithostratigraphic column of unit 3

and I1 in $\delta^{13}C_{org}$ concur with the overlying excursion in $\delta^{13}C_{carb}$ and $\delta^{18}O_{carb}$.

Discussion

The early Eocene is a time of global warmth. A eustatic sea level rise associated with the PETM is known globally. However, a causal link between the warming and transgression is not straightforward, because there are evidences of mismatch in their onset timings from some areas (Pujalte et al., 2014; Sluijs et al., 2008). The other early Eocene hyperthermal events are relatively less explored in comparison to the PETM. However, Sluijs et. al. (2008) reported a transgression from New Jersey, USA possibly linked to the ETM2. Sea-level curves published in recent times depict a sharp increase in the sea level near 54 Ma, and a higher sea level during the ETM2 than that corresponding to the PETM (Kominz et al., 2008; Miller et al., 2005, 2020).

On its long journey from the Southern Hemisphere to its current position in the Northern Hemisphere, the Indian plate was positioned on the palaeo-equator during the early Eocene. It collided shortly afterwards (~50 Ma) with the Eurasian plate. An anticlockwise rotation and a sudden slowdown of the tectonic plate are known to be associated with the collision (Copley et al., 2010).

These tectonic, climatic and eustatic situations form the backdrop of an exploration of the evolution of the Kutch Basin during the early Eocene.

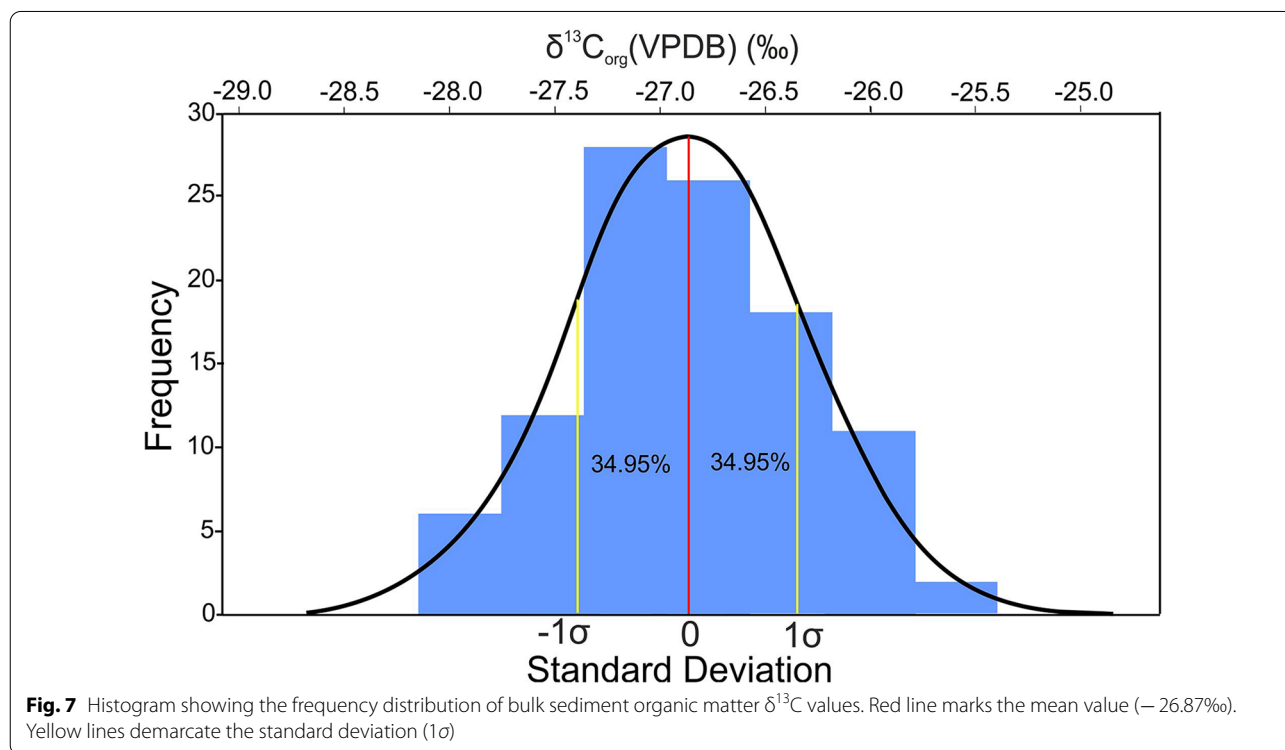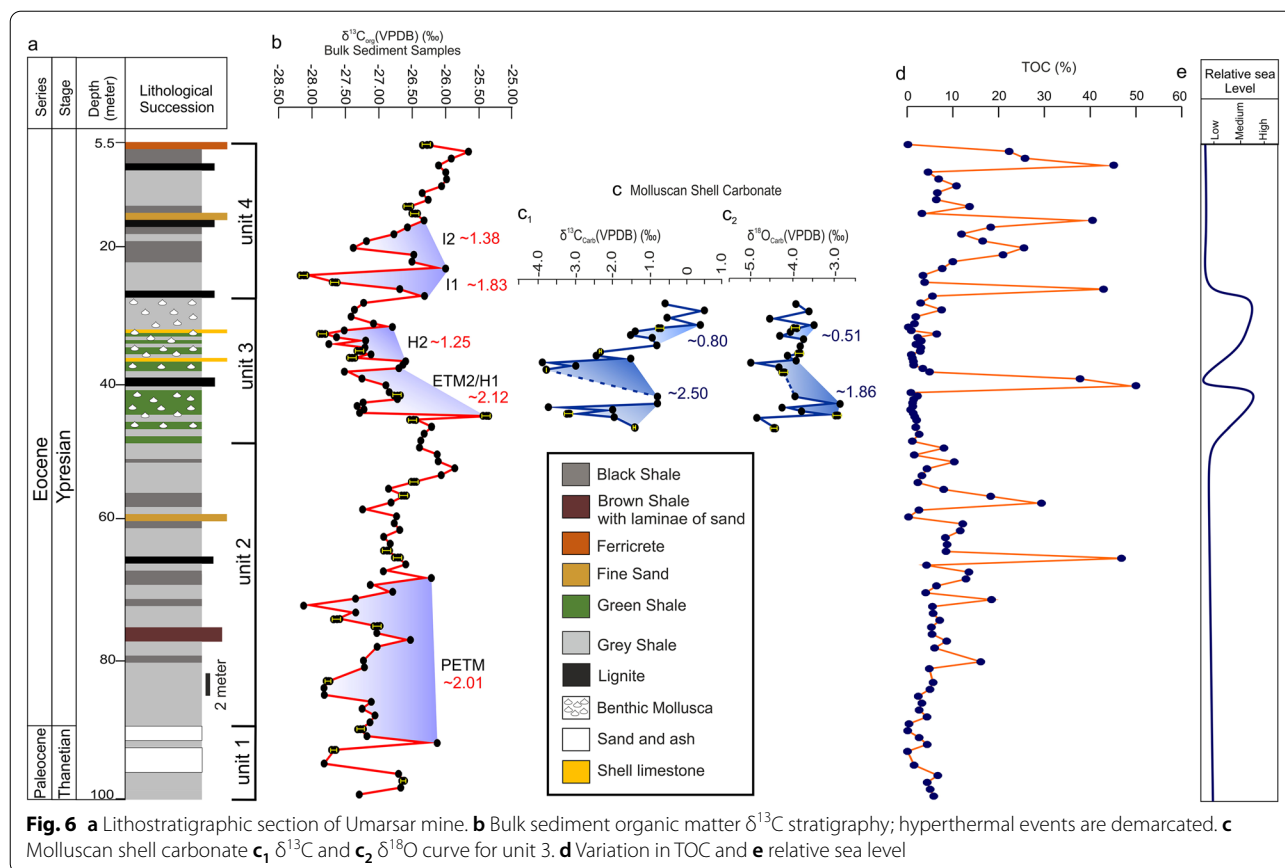## Stratigraphy and depositional environment

The overall plane-laminated, argillaceous succession in the studied section from the Umarsar mine of Kutch reflects a low-energy depositional environment. The presence of lignite and carbonaceous shale beds along with preserved plant remains and amber through the entire succession indicates the proximity of the basin to a forest-covered land. The green glauconitic shale with marine fossils in the middle of the succession represents a marine interval. Hence, the succession was developed in a coastal marginal marine setting. Pyrite is recovered from several levels including some from the green shale part, which indicates that the level of oxygen fluctuated in the basin.
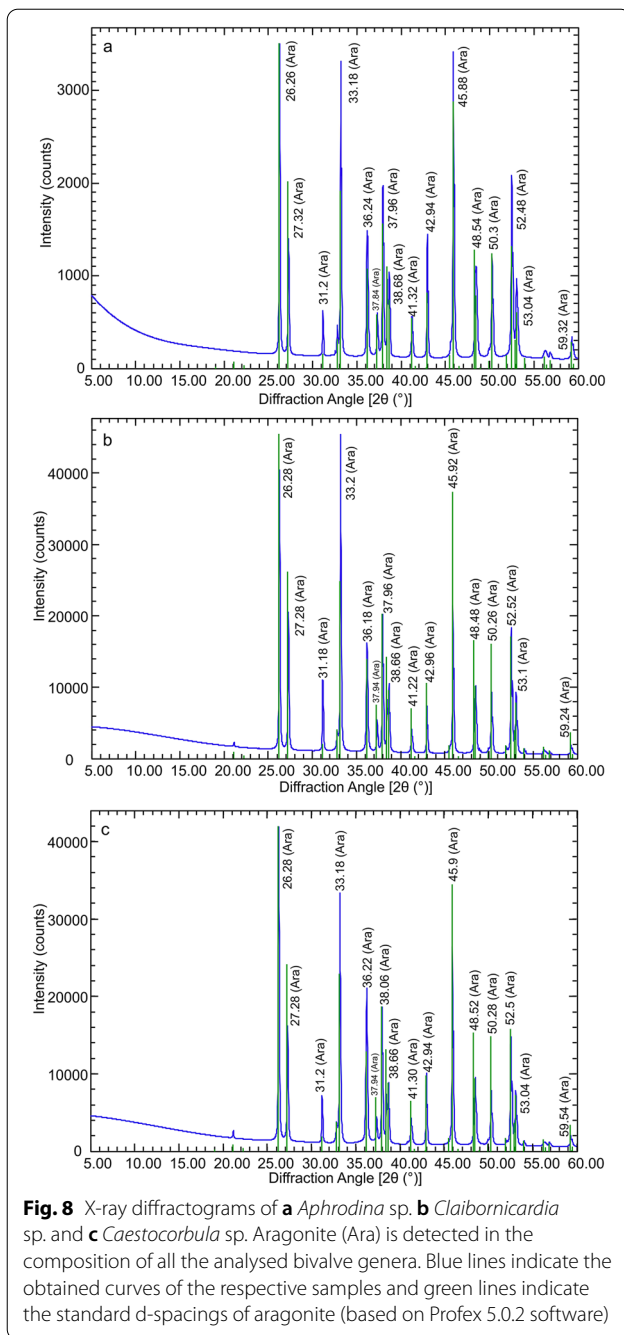
The unit 1, which contains pyroclastics and thin laminae of sandstones (Fig. 2), is a wash-over product from the Deccan Traps. This part is correlatable with the Matanomadh Formation (Biswas, 1992), which outcrops well in the Matanomadh area and is composed mainly of bright, variegated muds produced from pyroclastics and Deccan wash-overs.

The unit 2 is primarily an alternation of grey and carbonaceous black shale beds (Fig. 2). A 1 m thick lignite seam is also present in this part. The colours of these layers primarily reflect their organic carbon content. The grey shale contains the lowest and the lignite the highest amount of organic carbon (Fig. 6). The range of $\delta^{13}C_{org}$ values obtained from the succession indicates that the primary sources of organic carbon in this basin are C3 plants (Hare et al., 2018; Kohn, 2010). The deposition took place in a coastal swamp or lagoon that received sediments mainly from the weathering of terrestrial rocks. A recent geochemical analysis based on an 86 m drill core from the Matanomadh mine of Kutch Basin indicated a terrestrial source of organic carbon for the Naredi Formation (Chaudhuri et al., 2022). Palaeobotanical evidences vindicate the presence of a tropical forest in a coastal swamp, which was inundated by extreme tides (Mathews et al., 2018; Singh, 2021). The TOC content is dependent on the relative rate of accumulation of plant matter, i.e., the balance between the rate of accumulation of plant matter and the rate of sedimentation. A high rate of sediment supply would lower the TOC value. The relative rate of accumulation of plant matter depends mainly on the rate of precipitation. In the warm tropical climate of the time the hydrological cycle was intensified (Samanta et al., 2013, 2016). The black shale and lignite units represent phases of relatively low precipitation, which allowed accumulation of huge amount
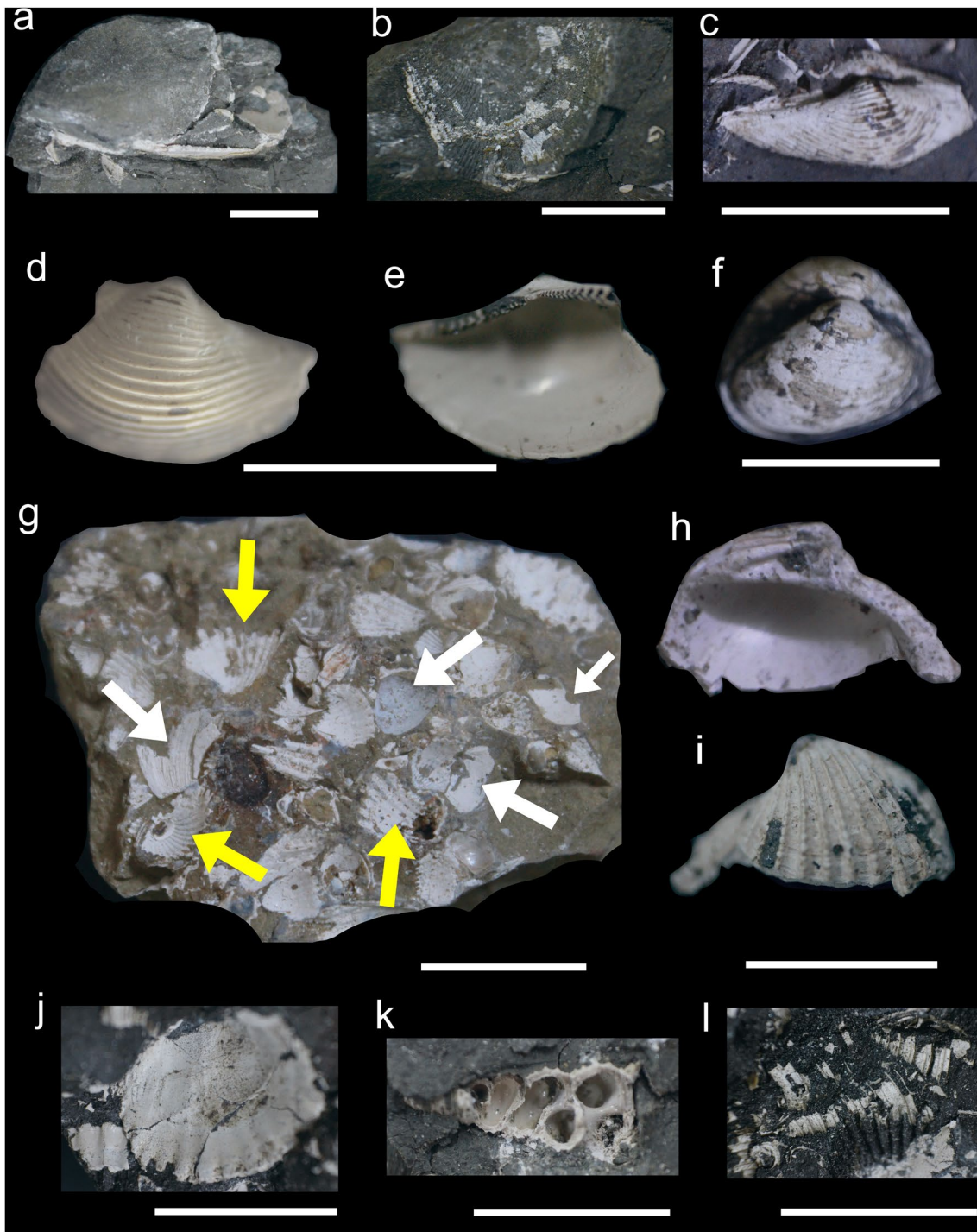
Fig. 5 Mollusc fossils from unit 3 **a** Broken shell of *Pteria* sp. **b** Partially preserved *Anomia* sp. **c**–**e** *Nuculana* sp. **c** within green shale, **d** external view of left valve, **e** internal view of left valve. **f** Articulated specimen of *Caestocorbula* sp. **g** *Aphrodina* sp. (white arrow) and *Claibornicardia* sp. (yellow arrow) in shell limestone **h**–**j** *Claibornicardia* sp. **h** internal view of left valve, **i** external view of left valve, **j** internal view of right valve. **k**, **l** *Turritella* sp. Scale bars 10 mm

Fig. 6 **a** Lithostratigraphic section of Umarsar mine. **b** Bulk sediment organic matter δ¹³C stratigraphy; hyperthermal events are demarcated. **c** Molluscan shell carbonate **c₁** δ¹³C and **c₂** δ¹⁸O curve for unit 3. **d** Variation in TOC and **e** relative sea level

Fig. 7 Histogram showing the frequency distribution of bulk sediment organic matter δ¹³C values. Red line marks the mean value (− 26.87‰). Yellow lines demarcate the standard deviation (1σ)

Fig. 8 X-ray diffractograms of **a** *Aphrodina* sp. **b** *Claibornicardia* sp. and **c** *Caestocorbula* sp. Aragonite (Ara) is detected in the composition of all the analysed bivalve genera. Blue lines indicate the obtained curves of the respective samples and green lines indicate the standard d-spacings of aragonite (based on Profex 5.0.2 software)

of plant matter. In contrast, a high precipitation resulted in intense weathering and high rate of sedimentation. However, the relationship between the rate of precipitation and the relative rate of accumulation of plant matter could be more complex. For example, a high precipitation would tend to encourage plant growth causing more plant-covered land area. This would diminish weathering. This argillaceous unit, i.e., unit 2, is more or less similar in nature to the lowermost part of the Gypseous

Shale Member of the Naredi Formation (Biswas, 1992). This part of the formation, however, does not contain any prominent lignite layer in the outcrop.

The unit 3 is primarily a green glauconitic shale unit bearing marine fossils and with intercalations of thin molluscan shell beds (Fig. 2). Glauconite forms only in very quiet marine waters with slow sedimentation, near the sediment–water interface, under a transgressive systems tract (TST) (Hesse & Schacht, 2011; Pietsch et al., 2016; Velde, 2014 and references therein). This interval was developed mostly below the wave base in a marine condition. The molluscs were found mainly from the green shale beds, and also from the shell beds. The shells are more fragmentary and concentrated in the shell beds. However, similar fossil forms as of the shale layers, whenever identifiable, are found from the shell beds. The shell beds formed at or above the wave base, under relatively agitated waters, which caused fragmentation of shells and winnowing of sediments (see also Samanta et al., 2016). It may be pointed out that glauconitic shell beds from the Eocene of Gulf Coastal Plain, USA are also commonly associated with TSTs and developed close to marginal marine environments (Pietsch et al., 2016).

The mollusc assemblage of the unit 3 is dominated by bivalves. A species of *Anomia* (family Anomiidae), along with *Pteria* sp. (family Pteriidae), are the most common forms in the lowermost part (Fig. 4). They are quickly followed up the sequence by members of Corbulidae (*Caestocorbula* sp.), Carditidae (*Claibornicardia* sp.) and Veneridae (*Aphrodina* sp.) (Fig. 4). These three forms are the most abundant in the marine interval. *Turritella* sp. appears in the upper part of unit 3 (Fig. 4). *Caestocorbula gujaratensis* Halder & Bano, 2015 and members of Carditidae (*Baluchicardia* and *Claibornicardia*) are also common in the early part of the marine mollusc bearing green shale layers of the Naredi Formation (Banerjee et al., 2019). Members belonging to these families also dominate the marine interval of the lignite-bearing succession of the Mangrol and other mines of the nearby Cambay Basin (personal observation; also Roy & Mukherjee, 2017). These corbulid and carditid bivalves along with some oysters and anomiids were the pioneers in the marine sequences of the early Paleogene in the western Indian basins (e.g., Halder & Mitra, 2021). Corbulids and anomiids, along with oysters are well-known representatives of marginal marine, often brackish, and sheltered environments, characterised by low selection pressure (Anderson, 2001; Bayne, 2017; Etim et al., 1998). Several corbulids including the extant *Corbula* are known to flourish in restricted, often hypoxic and polluted, environments as opportunists (Dominici, 2001; Etim et al., 1998). Corbulids are common, often the most predominant group, in the early Eocene marginal marine

muddy deposits from western India. Anomiids also have a wide range of salinity tolerance and are often associated with oysters, which are a well-known eurytopic group (Bayne, 2017; Castagna & Chanley, 1973). Pteriids can also tolerate wide range of salinities and prefer intertidal to subtidal waters (Gervis & Sims, 1992). Carditids commonly live in shallow burrows within muddy substrates (Coan & Valentich-Scott, 2012). The carditids found in this part of the succession represent early members of the "alticostate group" (Pérez, 2019). They preferred to live in very shallow burrows just below the sediment–water interface (McClure & Lockwood, 2015; Pérez, 2019) in shallow, subtidal parts of clastic-supported shelves (Dominici & Kowalke, 2007; Stanley, 1972). *Baluchicardia* and *Claibornicardia* are most common in the Eocene rocks of the Gulf Coastal Plain (Heaslip, 1968), where they are also often associated with glauconitic shales. Other molluscs recorded from this interval are *Aphrodina* sp. (family Veneridae), *Nuculana* sp. (Family Nuculanidae) and the only identifiable gastropod *Turritella* (family Turritellidae), and some unidentifiable fragments. *Aphrodina* and *Nuculana* are shallow-burrowing bivalves, living in soft-substratum shelf environment (Coan & Valentich-Scott, 2012; Moussavou, 2015). *Aphrodina* is an opportunist and known to form monospecific shell beds (Ahmad, 2005). Nuculanids, like corbulids, prefer a muddy, organic-rich substrate (Coan & Valentich-Scott, 2012). All these bivalves are commonly found in shallow, warm tropical seas (Coan & Valentich-Scott, 2012). *Turritella*, shallow-burrowing gastropod, generally prefers a shallow shelf with normal marine salinity and adequate supply of nutrients from upwelling or terrestrial sources (Allmon, 2011). While present-day representatives of *Turritella* prefer relatively cold waters early representatives from the Cretaceous and Paleogene were commonly known from warmer tropical areas (Allmon, 2011). The first to disperse in this part of the basin were epibenthic bivalves from anomiid and pteriid lineages. Later, with the establishment of a quiet marine environment, shallow burrowing bivalves and gastropods dominated the area. The predominance of eurytopic taxa and low diversity of the mollusc fauna indicate the prevalence of a restricted marginal marine environment.

The marine incursion during the deposition of this 3rd unit represents a transgression. The mollusc and benthic foraminifera bearing green shale in the middle to upper parts of the Gypseous Shale Member of the Naredi Formation mimics this succession. A similar succession with green shale beds containing marine molluscs and foraminifers is found in the Mangrol and Vastan mines of the nearby Cambay Basin (Clementz et al., 2011; Halder & Mitra, 2021; Samanta et al., 2013, 2016). Similar marine intervals have been recorded in most of the lignite mine sections of western India (see also Khozyem et al., 2021). This sedimentary motif of marine mollusc bearing green shale, sandwiched between lignite and carbonaceous shales, indicates the regional nature of the green shale unit and the transgression responsible for its deposition.

The unit 3 with marine molluscs can be correlated with fossiliferous parts of the outcrop sections of the Naredi Formation. The type section of the Naredi Formation is characterised by alternation between green shale and grey/brown shale in the lower part (Gypseous Shale Member). The green shale beds of this stratigraphic unit with marine molluscs and foraminifers occur a few meters above the base of the outcrop. Based on the presence of *Nummulites globulus nanus*, the green shale was assigned to SBZ 8 (Saraswati et al., 2012), which is ~54 Ma (Mochales et al., 2012; Serra-Kiel et al., 1998). The *Assilina* Limestone Member (Biswas, 1992), overlying the Gypseous Shale Member, was assigned to SBZ 11 based on its foraminiferal content, especially *Nummulites burdigalensis cantabricus* (Saraswati et al., 2012). An analysis of strontium isotopes (^{87}Sr/^{86}Sr) from foraminiferal tests also vindicates this age assignment (Anwar et al., 2013). Garg et. al. (2011) demonstrated a similar age range for the Gypseous Shale Member (~55–54 Ma or younger) based on its dinoflagellate assemblage. The green shale of the Naredi Formation commonly features bivalve specimens of *Caestocorbula gujaratensis* along with some carditid forms. In contrast, the mollusc assemblage from the overlying *Assilina* Limestone unit lacks these forms. The unit 3 of Umarsar mine section studied here is broadly correlatable with the Gypseous Shale Member. Having a similar lithology and mollusc assemblage the unit 3 is correlatable with the green shale from the middle-upper part of the Gypseous Shale Member. Therefore, the green shale of unit 3 from the Umarsar mine can be assigned to SBZ 8. The *Assilina* Limestone and its mollusc assemblage are absent in the mine section.

The unit 4 is dominantly composed of carbonaceous black shale and lignite beds (Fig. 2). A swampy/lagoonal condition resumed during the deposition of this unit. The relative rate of accumulation of plant matter was higher than that in the unit 2 as indicated by the predominance of layers with high TOC (Fig. 6, Additional file 1). A fine sandstone layer with sharp lower and upper surface contacts represents an event deposition (Fig. 2). The top is demarcated by a ferricrete (Fig. 2). This is likely to be equivalent to the lateritic top of the Naredi Formation, indicating subaerial exposure.

The succession encompassing the units 2 to 4 is lithologically equivalent to the Ypresian Naredi Formation (see also Singh, 2021). The outcrop of the formation mainly in and around the type section near the village

Nareda contains only thin lenses of lignite and black shale. The outcrop, in contrast to the mine section explored in this study, accommodates a prominent interval of limestone composed chiefly of the larger benthic foraminifera *Assilina*, The *Assilina* Limestone Member (Biswas, 1992). The absence of this unit, and the prevalence of lignite and carbonaceous shale layers in the Umarsar mine section indicate a relatively restricted nature of this part of the basin. The restricted nature is also evident by the presence of considerable quantity of pyrite, even in the marine green shale unit.

Isotope stratigraphy and hyperthermal events
$\delta^{13}C_{org}$

The range of $\delta^{13}C_{org}$ values obtained in this analysis varies between -25.40 and -28.15‰. The values show a normal distribution with a mean of -26.87‰ (Fig. 7). The stable isotopic studies so far carried out in different lignite mines from western Indian basins reported similar values (Agrawal et al., 2017; Clementz et al., 2011; Samanta et al., 2013). A very recent record reported $\delta^{13}C_{org}$ from five early Paleogene lignite mines of western India (Khozyem et al., 2021). It also reported similar values except from the Tadkeswar mine of the Cambay Basin, where the authors found a lower range of values. Our study on a lignitic sequence from the Cambay Basin also yielded similar values (Halder & Mitra, unpublished data). Agrawal et. al. (2017) and Khozyem et. al. (2021) reported $\delta^{13}C_{org}$ and its negative excursions from the Panandhro mine lying only about 5 km from Umarsar. Agrawal et. al. (2017) reported only the presence of ETM2, whereas Khozyem et. al. (2021) found the PETM and ETM2. Both these studies are based only on the upper 11–12 m of the succession, which became exposed by mining. The present study is the first to report $\delta^{13}C_{org}$ from the entire argillaceous sequence of the Umarsar mine having a thickness of 94.5 m, which rests on the Deccan Traps.

The range of $\delta^{13}C_{org}$ values obtained from the Umarsar mine falls in the range of modern C3 plants (Kohn, 2010). The palynological analyses carried out in all the Eocene lignite bearing successions of western India including the Kutch and Cambay basins of Gujarat, and the Barmer Basin of Rajasthan exhibit a prevalence of tropical C3 plant types, such as palm, dipterocarps etc. (e.g., Mathews et al., 2018; Paul et al., 2015; Sahay, 2011). Singh (2021) recently reported a similar palynological assemblage from the Umarsar mine.

The $\delta^{13}C_{org}$ curve from the data from the Umarsar mine succession exhibits five prominent negative excursions and a few smaller ones indicating hyperthermal events. The PETM at the boundary between the Paleocene and Eocene is globally the most widely documented

hyperthermal event, whereas studies on several other events are at a relatively early stage. Lauretano et. al. (2015) recorded six major negative CIEs after the PETM within the time period of 54 to 52 Ma, which correspond to ETM2, H2, I1, I2, J and ETM3. Among these hyperthermal events, the ETM2 and H2 are considered paired events, because only a small time gap separates them (Lauretano et al., 2015). The recorded time gaps between them ranges from 0.05 to 0.3 Ma. Similarly, the I1 and I2 are separated only by 0.15–0.2 Ma, and are paired. A time gap of ~0.4 Ma separates the two pairs (Lauretano et al., 2015; Westerhold et al., 2018). The reported ages of the PETM and ETM2 fall in the ranges of 55.93–55.53 Ma and 54.09–53.69 Ma (Westerhold et al., 2007, 2018), respectively. There is no independent age data available from the Umarsar mine. However, the fossiliferous green shale part of the section can be correlated with SBZ 8, which ranges in age from 54.7 to 53.4 Ma (Serra-Kiel et al., 1998; Mochales et al., 2012). There are two closely spaced CIEs in this interval separated by only 5.5 m of the succession. The older of this pair is preceded by the first CIE at an interval of 34 m. The younger of the pair is followed by the fourth CIE at an interval of 8.5 m. The last CIE is very close to the fourth and forms another pair with it. It appears, from the relative positions of the CIEs and distances between them, that the first CIE from the Umarsar mine succession is the PETM, which was followed by the paired hyperthermal events, ETM2–H2 and I1–I2. The ETM2–H2 pair is associated with the fossiliferous green shale part (Fig. 6).

The previous reports of EEH events from western India support this identification. Khozyem et. al. (2013) recorded the ETM2, albeit tentatively, from the marine fossil rich green shale part of the Gypseous Shale Member of the Naredi Formation, with which the green shale (unit 3) of the Umarsar mine has been correlated. The CIE associated with the ETM2 was initiated from the marine fossil bearing marl sandwiched between two main lignite seams of the Panandhro mine section also (Khozyem et al., 2021). The mines from the nearby Cambay Basin show a similar pattern of marine green shale occurring in the middle of a largely terrestrial lignite bearing succession. The ETM2 excursion initiated in this marine interval in most of these mines (Clementz et al., 2011; Khozyem et al., 2021; Samanta et al., 2013). Our analysis also yielded a similar $\delta^{13}C_{org}$ trajectory having paired CIEs from the green shale of the Mangrol mine of the Cambay Basin, preceded by one near the base of the mine and followed by another pair up the sequence (Halder & Mitra, unpublished data).

The first CIE, recorded from the lower part of the grey shale, i.e., unit 1 of the Umarsar mine, corresponds to the PETM. This CIE occurs in a relatively wide zone

containing two peaks and features a relatively small negative excursion compared to most other known PETM records of the world. Samanta et. al. (2013) reported a similar PETM, which corresponds to a thick stratigraphic interval of the Vastan mine from the Cambay Basin, Gujarat. The entire PETM, including initiation and recovery phases, represented by a thick sedimentary unit, is also known from other areas (e.g., Stassen et al., 2012). The value of the negative CIE (5.2‰) documented by Samanta et. al. (2013) from Cambay Basin, however, was higher than that we have recorded at Umarsar. The negative excursion associated with the PETM from the neighbouring Panandhro mine of Kutch (∼2‰) is however, consistent with our data (Khozyem et al., 2021). Khozyem et. al. (2021) also recorded similar short excursions from the Tadkeswar and Bhavnagar mines of the Cambay Basin.

The terrestrial sites commonly record a larger negative shift of $\delta^{13}C$ compared to the marine sites. The difference, however, essentially reflects the carbon archive analysed. Marine carbonates commonly show shorter CIEs than terrestrial and marine organic carbon (McInerney & Wing, 2011). However, there are a few terrestrial records from other parts of the world, which reported a short CIE. For example, the lignite bearing successions from Schoninger, Germany and Cobham, UK recorded negative CIEs of 2.6‰ and 3‰, respectively (Collinson et al., 2003; Lenz et al., 2021). A French record of the PETM also exhibits a relatively small negative excursion of 2.8‰ (Storme et al., 2012). These values of negative CIEs and also the peak values of $\delta^{13}C_{org}$ recorded from these basins are comparable to that recorded in the present study.

The magnitudes of the CIEs associated with the other hyperthermal events in our analysis are also often slightly lower than global terrestrial records. The terrestrial records of the ETM2 are few and the negative excursion ranges from 1.7 to 3.5‰ (Chen et al., 2014; Lenz et al., 2021). Our record of the negative excursion of the ETM2 (2.12‰) falls in the lower half of this range. The previously recorded excursions associated with the ETM2 from western Indian localities are, however, similar to ours (Agrawal et al., 2017; Khozyem et al., 2021; Samanta et al., 2013). The reports of other younger hyperthermal events from the terrestrial environment are fewer than that of the ETM2. The values of these negative CIEs are commonly slightly over 2‰, although lower values are also recorded (e.g., 1.6‰ from the Vastan mine, Cambay Basin, India; Samanta et al., 2013). We have recorded negative excursions of 1.25, 1.83 and 1.38‰ for the H2, I1 and I2, respectively.

A probable explanation of the short negative excursions of $\delta^{13}C_{org}$ from Umarsar is the possible mixing of organic matter (OM) from different areas with varied chemical natures. Mixing is common in a coastal transitional environment like the current study area, especially under an intensified hydrological cycle. The mixing could dampen the isotopic signatures. The water use efficiency of plants is affected by the salinity of water (Lomax et al., 2019). The $\delta^{13}C_{org}$ value of bulk OM, thus, can be affected as well by the changing salinity of the marginal marine setting of the Kutch Basin. $\delta^{13}C_{org}$ depends on several other factors, such as atmospheric pCO_2, mean annual precipitation, intensity of seasonality, decomposition of OM, etc. (Schubert & Jahren, 2012, 2013 and references therein; Kohn, 2010; Wang et al., 2015). Independent measures of the controlling factors are needed to assess their probable roles on $\delta^{13}C_{org}$, which are beyond the scope of this study. For example, the decomposition of OM depends on several factors, such as the quality of the litter, the redox potential of the environment, etc. The quality of the litter, in turn, is dependent on several factors, such as the ratio between carbon and nitrogen (C/N), the quantity of lignin and other components, etc. (Wang et al., 2015). So, future investigations are required to assess possible causes of the relatively short negative CIEs associated with the hyperthermal events here.

A sharp increase of $\delta^{13}C_{org}$ just before the equally sharp initial fall associated with the ETM2 is worth noticing (Fig. 6). We cannot explain this positive excursion with the present set of information available to us. Another short negative excursion midway between the PETM and ETM2 is present in our data (Fig. 6). A pre-ETM2 excursion has been recorded from a few other localities (D'Onofrio et al., 2016; Willard et al., 2019). We have also found a similar excursion from the Mangrol mine (Cambay Basin) data (Halder & Mitra, unpublished data).

$\delta^{13}C_{carb}$ and $\delta^{18}O_{carb}$

Marine carbonates from benthic and planktonic foraminifers are the most commonly analysed archives, used for recognition of EEH events (McInerney & Wing, 2011; Westerhold et al., 2018). While $\delta^{18}O$ from benthic foraminifers give palaeotemperatures of the sea floor, that from planktonic foraminifers is a proxy for the sea surface temperature. The measurement of $\delta^{18}O$ and $\delta^{13}C$ values from the same carbonate sample is the most frequently employed method in the studies for PETM and other EEHs. Such studies have so far been carried out commonly on marine sedimentary rocks, often derived from ocean drilling programmes of various Atlantic and Pacific sites. These drilled materials predominantly yield foraminifers. Hence, a plethora of isotopic studies on these organisms was done.

The marginal marine shales and claystones of our studied core did not yield any foraminifer specimen. We have found predominantly fragmentary mollusc shells from

most of the layers of unit 3. Shells of three bivalve species, *Claibornicardia* sp., *Caestocorbula* sp. and *Aphrodina* sp., have been analysed, because they are abundant at certain levels that almost cover the entire marine interval. The fossil shells retain pristine aragonite (Fig. 8, Additional file 2). This is the first report of $\delta^{18}O$ and $\delta^{13}C$ analyses on fossil benthic mollusc shells from the Cenozoic. A single species/genus analysis was not possible for the entire unit. Therefore, we relied on mixed species analysis. *Aphrodina* and *Claibornicardia* provided the bulk of samples for the lower and upper parts, respectively. The $\delta^{18}O_{carb}$ and $\delta^{13}C_{carb}$ values co-vary through the entire marine interval with more or less concurrent negative excursions, although mean $\delta^{13}C_{carb}$ exhibits a positive shift in the upper part of the interval (Fig. 6c). The CIEs in $\delta^{13}C_{org}$ and $\delta^{13}C_{carb}$ coincide with the negative excursions of $\delta^{18}O$ (Fig. 6b, c). These features reflect the robustness of this record in spite of the use of mixed species in the analyses. The negative excursions of $\delta^{18}O$ along with $\delta^{13}C_{org}$ and $\delta^{13}C_{carb}$ indicate warming events during the marine interval of the Umarsar section caused by the injection of a large quantity of lighter carbon. This general conformity of isotope data from carbonate and organic carbon supports the recognition of CIEs in $\delta^{13}C_{org}$ beyond the marine interval as representing hyperthermal events.

The negative excursions recorded from many areas of the world are strongly variable. The magnitude of the ETM2 CIE we report here from benthic mollusc carbonate is relatively higher than most of the recorded data from marine benthic, planktonic or bulk carbonates (e.g., Barnet et al., 2019; Coccioni et al., 2012; Cui & Schubert, 2017; D'haenens et al., 2014; D'Onofrio et al., 2016; Galeotti et al., 2010; Leon-Rodriguez & Dickens, 2010; Lourens et al., 2005; Slotnick et al., 2012; Westerhold et al., 2018). The $\delta^{13}C_{carb}$ values are also, on an average, more depleted in ^{13}C in our analysis than marine foraminiferal carbonate values. The $\delta^{18}O_{carb}$ values are also more negative than global records, although the magnitudes of excursions are comparable to other reports.

The $\delta^{13}C_{carb}$ value is primarily a function of the dissolved inorganic carbon (DIC) of the water. A small value indicates enrichment of lighter carbon in DIC. In the open pelagic part of the oceans $\delta^{13}C_{DIC}$ decreases with depth, because ^{12}C-enriched organic matter descends to the deep, where its oxidation releases lighter carbon enriched CO_2 (Katz et al., 2010). In the quiet shallow marine environment of the Kutch Basin, adjacent to a swamp, terrestrial plant derived organic matter was never in short supply. Its oxidation would enrich the DIC with ^{12}C. Terrestrial C3 plants commonly have lower $\delta^{13}C$ than marine phytoplanktons (Kumar et al., 2016 and references therein). This is also reflected in the low $\delta^{13}C$ values of mollusc carbonate from this marginal marine setting. The low values of $\delta^{18}O$ were also resulted from mixing of fresh and marine waters. The freshwater has a lower $\delta^{18}O$ than marine water (Katz et al., 2010; Wright, 2001). Diagenesis can alter isotopic signatures to a certain extent. However, the diagenetic effect on the analysed mollusc shells is negligible in a clay-dominated depositional environment. Pristine aragonitic shells are preserved as revealed from the XRD analysis (Fig. 8). There can be other factors, especially related to difference in fractionation by different organisms. Species-specific difference in fractionation by benthic and planktonic foraminifers is widely appreciated (Katz et al., 2010 and references therein). Whether molluscs broadly differ in isotopic signatures from foraminifers needs to be explored in future.

The positive shift of $\delta^{13}C_{carb}$ curve after the ETM2, which is not reflected in $\delta^{18}O_{carb}$ curve (Fig. 6c), is intriguing. This may happen due to several factors, a few of which are discussed here. (1) Differences in species-specific isotope fractionation may be important. Interspecific fractionation is significantly more variable in carbon isotopes than oxygen isotopes (Lécuyer et al., 2004). These authors demonstrated only negligible fractionation differences in oxygen isotopes between different recent mollusc species from a tropical basin. (2) Microhabitats within the benthic habitat differ in geochemical environments and hence, the shells that grow in different microhabitats differ in isotope signatures. This is especially pronounced in carbon isotope fractionation between epi- and infaunal forms, and also between shallow- and deep-infaunal forms. The $\delta^{13}C_{DIC}$ is lower within the sediment layer than on the substrate because of the oxidation of organic matter inside the sediment (Katz et al., 2010). It further decreases with sediment depth (Katz et al., 2010). In an organic rich sedimentary environment of the marginal marine setting, as in the studied section, this factor might have played an important role. *Aphrodina*, which is primarily used for the isotope analysis for the lower part of the marine interval of the Umarsar mine section, has the potential to live in relatively deeper burrows than *Claibornicardia*. The former is more elongated and has a deeper pallial sinus than the latter. The latter was chiefly used for the isotope analysis for the upper part of the interval. (3) The marine influence might have increased in the upper part of the section than in the lower part. This change is also likely to influence carbon isotope ratios more than oxygen isotope ratios (Lécuyer et al., 2004). One or more of these factors may be responsible for the difference in oxygen and carbon isotope signatures from the upper part of the marine interval of this mine section. A proper appraisal of the

proximal cause requires future studies on interspecific differences in isotopic signatures of benthic molluscs.

Hyperthermal and transgressive events

A transgression associated with the PETM is documented globally in areas dispersed from high southern to high northern latitudes and palaeo-tropics (Gibson et al., 1993; Harding et al., 2011; Pujalte et al., 2014; Schulte et al., 2011; Sluijs et al., 2008, 2011, 2014; Speijer & Morsi, 2002). Transgressions were recorded based on sedimentological and palynological evidences. However, the causal link between the PETM and transgression are not straightforward as evidenced from some areas. For instance, the New Jersey shelf, USA recorded a transgression 20–200ky prior to the PETM (Sluijs et al., 2008). The sea level continued to rise during and after the PETM (Pujalte et al., 2014). Ambiguity also prevails regarding the causes of the transgression on two accounts. First, it is generally believed that the earth lacked a cryosphere during the Paleocene–Eocene. However, only a thermal expansion of water could not account for the extent of transgression coincident with the PETM (Sluijs et al., 2008; Speijer & Morsi, 2002). Hence, the thermal expansion of water and the melting of a possible thin Antarctic ice cover have been invoked by researchers to explain this transgression (Miller et al., 2005, 2011; Sluijs et al., 2008; Speijer & Morsi, 2002). Second, an initiation of the transgression before the PETM also calls for a mechanism other than those related to warming. Tectonism and volcanism, especially related to the North Atlantic Igneous Province, were proposed to have played some roles in this transgression (Pujalte et al., 2014; Sluijs et al., 2008). However, the global nature of the transgression and common coincidence with the PETM are generally considered as an indication of the eustatic rise related to the warming (Sluijs et al., 2008, 2014).

The other early Eocene hyperthermal (EEH) events are much less studied from this point of view. However, Sluijs et. al. (2008) tentatively associated the palynological and sedimentological evidences from a slightly younger stratigraphic level in New Jersey, USA and some other sites with a later transgression related to the ETM2 or another temporally close hyperthermal event (see also Willard et al., 2019). There is, so far, no other report of a transgression associated with any other hyperthermal events of the early Eocene.

The first ever reported EEH from the Indian subcontinent, ETM2 from the Vastan mine of the Cambay Basin, falls within the marine interval (Clementz et al., 2011). Our unpublished data also revealed the ETM2–H2 pair from within the marine interval of the Mangrol mine, adjacent to the Vastan mine (Halder & Mitra, unpublished data). Other studies often revealed the initiation

of the CIE associated with the ETM2 within the marine interval, whereas the peak within the lignite seam overlying it, in the Kutch and Cambay basins (Khozyem et al., 2021).

The present study documents the PETM from a primarily coastal terrestrial setting. Here, the PETM is followed by the first lignite seam of the Umarsar mine. Marine inundation of the basin coincident with the PETM, if any, was not reflected in the rocks from this part of the basin. However, a transgression, demarcated by the appearance of marine mollusc bearing layers, is associated here with the pair of EEH events of ETM2 and H2. The marine inundation began slightly before the onset of the CIE associated with the ETM2 and retreats after the end of the CIE of H2 (Fig. 6). The marine sedimentary units appear to precede the CIEs on both the occasions. This pattern is consistent with the transgressions associated with the PETM reported from several areas of the world, where sedimentary and palaeontological evidences of transgression in the rock record appear slightly before the negative excursion of $\delta^{13}C$ (Sluijs et al., 2008, 2011). Such offset between the transgression and the biochemical response of warming led to invoking association of other local or regional factors with the transgression. The offset, now documented also for the ETM2 and H2, needs further attention. There are reports of warming preceding the PETM (Secord et al., 2010; Sluijs et al., 2007). Future research should be directed to documenting if this offset is global in nature and also associated with other hyperthermal events.

The association of the Ypresian transgression and ETM2–H2 hyperthermal pair in two contiguous basins of western India suggests a causal link between these events. However, the absence of any marine incursion related to the PETM, which is a stronger warming event than the ETM2–H2, and somewhat irregular position of the latter hyperthermal events with respect to the marine interval in the lignite mines make the relationship slightly ambiguous. A detailed regional correlation of the western Indian basins with respect to the hyperthermal events and marine incursion is needed to confirm the purported relationships. This study is a part of the bigger plan of such a regional survey. The recent report by Khozyem et. al. (2021) strongly suggests the regional nature of the association between the transgression and the hyperthermal events.

The recently published global mean sea level (GMSL) curve based on $\delta^{18}O$ from the Pacific benthic foraminifers and Ca/Mg estimates (Miller et al., 2020) reveals a sharp increase in the sea level and a higher sea level near ~ 54 Ma than that near the P–E boundary at 56 Ma. Other sea level curves obtained earlier by 'backstripping' estimates from continental margins (Kominz et al., 2008;

Miller et al., 2005) also support this. The current consensus about the ages of the PETM and ETM2 are 56 Ma and 54.09 Ma, respectively (Westerhold et al., 2018). Hence, the transgression recorded in the Kutch and Cambay basins reflect a global event. Only this high elevation of the sea could inundate this coastal and largely terrestrial basins, whereas the earlier shorter rise of the water level was not registered here (Fig. 6e). A global increase in the mean sea level requires a global cause. The coeval global warming due to the ETM2–H2 pair is the strongest candidate in explaining this transgression.

Alternatively, or additionally, tectonism could be responsible for the transgression. The Indian plate was going through a phase of strong tectonic activity during the Paleogene. The Indian plate collided with the Tibetan plate in the Ypresian after a long journey from the southern hemisphere since the Cretaceous. The collision was accompanied by a sudden slowdown of the plate movement (Copley et al., 2010). The western Indian basins could have experienced the transgression due to this sudden slowdown in a manner similar to a vehicle that experiences sudden gusts of wind on its rear with sudden brake in speed. An anticlockwise sense of rotation of the Indian plate might also have played some roles in the transient Ypresian transgression on its western margin. The onset timing of the collision and mechanisms involved in the suturing of the two plates are, however, strongly debated. The documented age of the collision falls anywhere between the Late Cretaceous and Oligo–Miocene (Hu et al., 2016). Most recent researches put the onset at 61–56 Ma (An et al., 2021; Jadoon et al., 2021). However, the main collision event is often considered to have taken place around 50 Ma (e.g., Copley et al., 2010; Patriat & Achache, 1984), which post-dates the transgression. It is difficult to conclusively link the tectonic factor with the transgression at the present state of knowledge about the timing. Furthermore, the global nature of the transgression is difficult to accommodate in this tectonic scenario.

Conclusions

The early Eocene sedimentary rocks containing lignite from the Umarsar mine, Kutch, western India have been analysed from sedimentological, palaeontological and geochemical aspects. The deposition took place primarily in a coastal marginal marine environment. The $\delta^{13}C_{org}$ data depicts five negative excursions, which have been identified as the PETM, ETM2/H1, H2, I1 and I2 from an older to younger sequence based on their stratigraphic positions and relative distances. The trajectories of $\delta^{13}C_{carb}$ and $\delta^{18}O_{carb}$ from pristine shells of molluscs, derived from the middle part of the succession, conform

to $\delta^{13}C_{org}$ in that interval and reveal two hyperthermal events. This marine interval is correlatable to a similar interval from the outcrop of the Kutch Basin, which was constrained to SBZ8. The two hyperthermal events from this part of the succession have been identified as ETM2 and H2. The discovery of the early Eocene hyperthermal events from Kutch is important, because most of the available reports of the EEH are from marine sequences of relatively high latitudes, whereas the present one comes from a marginal marine transitional environment of a tropical basin. The study finds the co-occurrence of ETM2 and H2 with the marine incursion. This association appears to be regionally valid, which suggests a causal link. It is also supported by the global mean sea level curves. Future studies from other parts of the world need to be directed towards it for the confirmation.

There are several scientific questions that need to be addressed in future. For example, the discrepancy in GMSL coeval to the PETM and ETM2 is intriguing, because the former is a stronger warming event than the latter. The fact that the sea water responded to the warming before the negative shift of $\delta^{13}C_{org}$ also requires attention from future studies, if warming events were solely responsible for the transgressions. The presence of two or more pulses in a hyperthermal event is an interesting feature that also needs attention from future investigators. This study, being the first to report $\delta^{13}C$ and $\delta^{18}O$ from benthic molluscs, cannot be compared with other records of early Eocene. Global records are seriously biased towards foraminiferal carbonates. Future studies need to carry out isotopic analyses on molluscs and other carbonate sources than foraminifers.

Abbreviations
CARB: Carbonate; CIE: Carbon isotope excursion; DIC: Dissolved inorganic carbon; CF–IRMS: Continuous Flow–Isotope Ratio Mass Spectrometry; EA–IRMS: Elemental Analyser–Isotope Ratio Mass Spectrometry; EEH: Early Eocene hyperthermal; ETM: Eocene thermal maximum; GMSL: Global mean sea level; IAEA: International Atomic Energy Agency; LBF: Larger benthic foraminifer; MFZ: Maximum flooding zone; OM: Organic matter; PETM: Paleocene Eocene thermal maximum; SBZ: Shallow benthic zone; TOC: Total organic carbon; VPDB: Vienna Pee Dee Belemnite; XRD: X-ray diffraction.

Supplementary Information
The online version contains supplementary material available at https://doi.org/10.1186/s13358-022-00255-1.

> **Additional file 1.** Results of geochemical analyses on drill-core samples from Umarsar mine, Kutch, western India. **Table S1.** (a) TOC and $\delta^{13}C_{org}$ from bulk sediment samples. (b) $\delta^{13}C_{carb}$ and $\delta^{18}O_{carb}$ from molluscan shells. **Table S2.** (a) $\delta^{13}C$ of control samples for analysis of bulk sediment samples. (b) $\delta^{13}C$ and $\delta^{18}O$ of control samples for analyses of molluscan carbonate samples.
>
> **Additional file 2.** Results of XRD analysis on three bivalve shells from Umarsar mine, Kutch, western India.

References

Agrawal, S., Verma, P., Rao, M. R., Garg, R., Kapur, V. V., & Bajpai, S. (2017). Lignite deposits of the Kutch Basin, western India: Carbon isotopic and palynological signatures of the early Eocene hyperthermal event ETM2. *Journal of Asian Earth Sciences, 146*, 296–303.

Ahmad, F. (2005). The heterodont bivalve *Aphrodina dutrugei* (Cocquand, 1862) from the Cenomanian of Jordan. *Revista Italiana di Paleontologia e Stratigrafia., 111*, 191–195.

Allmon, W. D. (2011). Natural history of turritelline gastropods (Cerithioidea: Turritellidae): A status report. *Malacologia, 54*, 159–202.

An, W., Hu, X., Garzanti, E., Wang, J. G., & Liu, Q. (2021). New precise dating of the India-Asia collision in the Tibetan Himalaya at 61 Ma. *Geophysical Research Letters, 48*(3), e2020GL090641. https://doi.org/10.1029/2020GL090641

Anderson, L. C. (2001). Temporal and geographic size trends in Neogene Corbulidae (Bivalvia) of tropical America: Using environmental sensitivity to decipher causes of morphologic trends. *Palaeogeography, Palaeoclimatology, Palaeoecology, 166*(1–2), 101–120.

Anwar, D., Choudhary, A. K., & Saraswati, P. K. (2013). Strontium isotope stratigraphy of the Naredi Formation, Kutch Basin, India. *Geological Society of India, Special Publication, 1*, 298–306.

Bajpai, S., Kapur, V. V., Das, D. P., Tiwari, B. N., Saravanan, N., & Sharma, R. (2005). Early Eocene land mammals from the Vastan Lignite Mine, District Surat (Gujarat), western India. *Journal of the Palaeontological Society of India, 50*(1), 101–113.

Bajpai, S., & Thewissen, J. G. M. (2002). Vertebrate fauna from Panandhro lignite field (lower Eocene), District Kachchh, western India. *Current Science, 82*(5), 507–509.

Banerjee, S., Das, S., Halder, K., & Chakrabarti, N. (2019). Palaeoecological analysis of Benthic Molluscs from the Eocene of Kutch, Gujarat reveals an event of storm induced concentration of shells in a quiet marginal marine environment. *Journal of the Geological Society of India, 94*(2), 162–170.

Banerjee, S., Khanolkar, S., & Saraswati, P. K. (2018). Facies and depositional settings of the Middle Eocene-Oligocene carbonates in Kutch. *Geodinamica Acta, 30*, 119–136. https://doi.org/10.1080/09853111.2018.1442609

Barnet, J. S., Littler, K., Westerhold, T., Kroon, D., Leng, M. J., Bailey, I., Röhl, U., & Zachos, J. C. (2019). A high-fidelity benthic stable isotope record of late Cretaceous–early Eocene climate change and carbon-cycling. *Paleoceanography and Paleoclimatology, 34*(4), 672–691.

Bayne, B. L. (2017). *Biology of oysters*. Academic Press.

Biswas, S. K. (1992). Tertiary stratigraphy of Kutch. *Journal of the Palaeontological Society of India, 37*, 1–29.

Biswas, S. K. (2005). A review of structure and tectonics of Kutch basin, western India, with special reference to earthquakes. *Current Science, 88*(10), 1592–1600.

Castagna, M., & Chanley, P. (1973). Salinity tolerance of some marine bivalves from inshore and estuarine environments in Virginia waters on the western mid-Atlantic coast. *Malacologia, 12*, 47–96.

Catuneanu, O., & Dave, A. (2017). Cenozoic sequence stratigraphy of the Kachchh Basin, India. *Marine and Petroleum Geology, 86*, 1106–1132.

Chaudhuri, S., De, S., Srivastava, H., Chattopadhyay, K., & Bhaumik, A. K. (2022). Multiproxy analysis constraining climatic control over the Cenozoic depositional history of Kachchh, Western India. *Geological Journal*. https://doi.org/10.1002/gj.4511

Chen, Z., Ding, Z., Tang, Z., Wang, X., & Yang, S. (2014). Early Eocene carbon isotope excursions: Evidence from the terrestrial coal seam in the Fushun Basin, Northeast China. *Geophysical Research Letters, 41*(10), 3559–3564.

Clementz, M., Bajpai, S., Ravikant, V., Thewissen, J. G. M., Saravanan, N., Singh, I. B., & Prasad, V. (2011). Early Eocene warming events and the timing of terrestrial faunal exchange between India and Asia. *Geology, 39*(1), 15–18.

Coan, E. V., & Valentich-Scott, P. (2012). *Bivalve seashells of tropical west America* (Vol. 1258). Santa Barbara Museum of Natural History.

Coccioni, R., Bancalà, G., Catanzarit, R., Fornaciari, E., Frontalini, F., Giusberti, L., Jovane, L., Luciani, V., Savian, J., & Sprovieri, M. (2012). An integrated stratigraphic record of the Palaeocene–lower Eocene at Gubbio (Italy): New insights into the early Palaeogene hyperthermals and carbon isotope excursions. *Terra Nova, 24*(5), 380–386.

Collinson, M. E., Hooker, J. J., & Grocke, D. R. (2003). Cobham lignite bed and penecontemporaneous macrofloras of southern England: A record of vegetation and fire across the Paleocene–Eocene thermal maximum. Geological society of America special paperIn S. L. Wing, P. D. Gingerich, B. Schmitz, & E. Thomas (Eds.), *Causes and consequences of globally warm climates in the Early Paleogene* (Vol. 369, pp. 333–349). Geological Society of America.

Copley, A., Avouac, J. P., & Royer, J. Y. (2010). India-Asia collision and the Cenozoic slowdown of the Indian plate: Implications for the forces driving plate motions. *Journal of Geophysical Research: Solid Earth, 115*, B03410. https://doi.org/10.1029/2009JB006634

Cui, Y., & Schubert, B. A. (2017). Atmospheric pCO_2 reconstructed across five early Eocene global warming events. *Earth and Planetary Science Letters, 478*, 225–233.

D'haenens, S., Bornemann, A., Claeys, P., Röhl, U., Steurbaut, E., & Speijer, R. P. (2014). A transient deep-sea circulation switch during Eocene thermal maximum 2. *Paleoceanography, 29*(5), 370–388.

Dickens, G. R., Castillo, M. M., & Walker, J. C. (1997). A blast of gas in the latest Paleocene: Simulating first-order effects of massive dissociation of oceanic methane hydrate. *Geology, 25*(3), 259–262.

Dickens, G. R., O'Neil, J. R., Rea, D. K., & Owen, R. M. (1995). Dissociation of oceanic methane hydrate as a cause of the carbon isotope excursion at the end of the Paleocene. *Paleoceanography, 10*(6), 965–971.

Doebelin, N., & Kleeberg, R. (2015). Profex: A graphical user interface for the Rietveld refinement program BGMN. *Journal of Applied Crystallography, 48*(5), 1573–1580.

Dominici, S. (2001). Taphonomy and paleoecology of shallow marine macrofossil assemblages in a collisional setting (Late Pliocene–Early Pleistocene, western Emilia, Italy). *Palaios, 16*, 336–353.

Dominici, S., & Kowalke, T. (2007). Depositional dynamics and the record of ecosystem stability: Early Eocene faunal gradients in the Pyrenean foreland, Spain. *Palaios, 22*, 268–284. https://doi.org/10.2110/palo.2005.p05-022r

D'Onofrio, R., Luciani, V., Fornaciari, E., Giusberti, L., Boscolo Galazzo, F., Dallanave, E., Westerhold, T., Sprovieri, M., & Telch, S. (2016). Environmental perturbations at the early Eocene ETM2, H2, and I1 events as inferred by Tethyan calcareous plankton (Terche section, northeastern Italy). *Paleoceanography, 31*(9), 1225–1247.

Etim, L., Sankare, Y., Brey, T., & Arntz, W. (1998). Dynamics of unexploited population of Corbula trigona (Bivalvia: Corbulidae) in a brackish-water lagoon, Cote D'Ivoire. *Archive of Fishery and Marine Research, 46*(3), 253–262.

Folie, A., Rana, R. S., Rose, K. D., Sahni, A., Kumar, K., Singh, L., & Smith, T. (2012). Early Eocene frogs from vastan lignite mine, Gujarat, India. *Acta Palaeontologica Polonica, 58*(3), 511–524.

Galeotti, S., Krishnan, S., Pagani, M., Lanci, L., Gaudio, A., Zachos, J. C., Monechi, S., Morelli, G., & Lourens, L. (2010). Orbital chronology of Early Eocene hyperthermals from the Contessa Road section, central Italy. *Earth and Planetary Science Letters, 290*(1–2), 192–200.

Garg, R., Ateequzzaman, K., Prasad, V., Tripathi, S. K. M., Singh, I. B., Jauhri, A. K., & Bajpai, S. (2008). Age-diagnostic dinoflagellate cysts from the lignite-bearing sediments of the Vastan lignite mine, Surat District, Gujarat, western India. *Journal of the Palaeontological Society of India, 53*(1), 99–105.

Garg, R., Prasad, V., Thakur, B., Singh, I. B., & Khowaja-Ateequzzaman. (2011). Dinoflagellate cysts from the Naredi Formation, southwestern Kutch, India: Implication on age and palaeoenvironment. *Journal of the Palaeontological Society of India, 56*(2), 201–218.

Gervis, M. H., & Sims, N. A. (1992). *The biology and culture of pearl oysters (Bivalvia: Pteriidae)* (pp. 1–49). International Center for Living Aquatic Resources Management Studies and Reviews.

Gibson, T. G., Bybell, L. M., & Owens, J. P. (1993). Latest Paleocene lithologic and biotic events in neritic deposits of southwestern New Jersey. *Paleoceanography, 8*(4), 495–514.

Giusberti, L., Rio, D., Agnini, C., Backman, J., Fornaciari, E., Tateo, F., & Oddone, M. (2007). Mode and tempo of the Paleocene–Eocene thermal maximum in an expanded section from the Venetian pre-Alps. *Geological Society of America Bulletin, 119*(3–4), 391–412.

Halder, K., & Das, S. (2019). New subfamily Indovolutinae and other volutids (Volutidae, Gastropoda) from the Eocene of Kutch, western India and their paleobiogeographic implications. *Journal of Paleontology, 93*(5), 899–915.

Halder, K., & Mitra, A. (2021). Facultative monogamy in an early Eocene brooding oyster and its evolutionary implications. *Acta Palaeontologica Polonica, 66*(3), 647–662.

Harding, I. C., Charles, A. J., Marshall, J. E., Pälike, H., Roberts, A. P., Wilson, P. A., Jarvis, E., Thorne, R., Morris, E., Moremon, R., & Pearce, R. B. (2011). Sea-level and salinity fluctuations during the Paleocene–Eocene thermal maximum in Arctic Spitsbergen. *Earth and Planetary Science Letters, 303*(1–2), 97–107.

Hare, V. J., Loftus, E., Jeffrey, A., & Ramsey, C. B. (2018). Atmospheric CO_2 effect on stable carbon isotope composition of terrestrial fossil archives. *Nature Communications, 9*, 252. https://doi.org/10.1038/s41467-017-02691-x

Heaslip, W. G. (1968). Cenozoic evolution of the alticostate venericards in Gulf and East Coastal North America. *Palaeontographica Americana, 6*, 55–135.

Hesse, R., & Schacht, U. (2011). Early diagenesis of deep-sea sediments. *Developments in Sedimentology, 63*, 557–713.

Höntzsch, S., Scheibner, C., Guasti, E., Kuss, J., Marzouk, A. M., & Rasser, M. W. (2011). Increasing restriction of the Egyptian shelf during the Early Eocene?—New insights from a southern Tethyan carbonate platform. *Palaeogeography, Palaeoclimatology, Palaeoecology, 302*(3–4), 349–366.

Hu, X., Garzanti, E., Wang, J., Huang, W., An, W., & Webb, A. (2016). The timing of India-Asia collision onset–Facts, theories, controversies. *Earth-Science Reviews, 160*, 264–299.

Jadoon, U. F., Huang, B., Shah, S. A., Rahim, Y., Khan, A. A., & Bibi, A. (2021). Multi-stage India-Asia collision: Paleomagnetic constraints from Hazara-Kashmir syntaxis in the western Himalaya. *GSA Bulletin*. https://doi.org/10.1130/B36116.1

Katz, M. E., Cramer, B. S., Franzese, A., Hönisch, B., Miller, K. G., Rosenthal, Y., & Wright, J. D. (2010). Traditional and emerging geochemical proxies in Foraminifera. *Journal of Foraminiferal Research, 40*(2), 165–192.

Khanolkar, S., & Saraswati, P. K. (2019). Eocene foraminiferal biofacies in Kutch Basin (India) in context of palaeoclimate and palaeoecology. *Journal of Palaeogeography, 8*(1), 1–16.

Khozyem, H., Adatte, T., Keller, G., & Spangenberg, J. E. (2021). Organic carbon isotope records of the Paleocene–Eocene thermal maximum event in India provide new insights into mammal origination and migration. *Journal of Asian Earth Sciences, 212*, 104736.

Khozyem, H., Adatte, T. H., Keller, G., Spangenberg, J. E., Saravanan, N., & Bajpai, S. (2013). Paleoclimate and Paleoenvironment of the Naredi Formation (Early Eocene), Kutch, Gujarat, India. *Geological Society of India Special Publication, 1*, 165–182.

Kohn, M. J. (2010). Carbon isotope compositions of terrestrial C3 plants as indicators of (paleo) ecology & (paleo) climate. *Proceedings of the National Academy of Sciences, 107*(46), 19691–19695.

Kominz, M. A., Browning, J. V., Miller, K. G., Sugarman, P. J., Mizintseva, S., & Scotese, C. R. (2008). Late Cretaceous to Miocene sea-level estimates from the New Jersey and Delaware coastal plain coreholes: An error analysis. *Basin Research, 20*(2), 211–226.

Kumar, K., Rana, R. S., & Singh, H. (2007). Fishes of the Khuiala Formation (Early Eocene) of the Jaisalmer Basin, Western Rajasthan, India. *Current Science, 93*, 553–559.

Kumar, V., Tiwari, M., Nagoji, S., & Tripathi, S. (2016). Evidence of anomalously low $\delta^{13}C$ of marine organic matter in an Arctic fjord. *Scientific Reports, 6*, 36192. https://doi.org/10.1038/srep36192

Lauretano, V., Littler, K., Polling, M., Zachos, J. C., & Lourens, L. J. (2015). Frequency, magnitude and character of hyperthermal events at the onset of the Early Eocene Climatic Optimum. *Climate of the Past, 11*(10), 1313–1324.

Lécuyer, C., Reynard, B., & Martineau, F. (2004). Stable isotope fractionation between mollusc shells and marine waters from Martinique Island. *Chemical Geology, 213*(4), 293–305.

Lenz, O. K., Montag, M., Wilde, V., Methner, K., Riegel, W., & Mulch, A. (2021). Early Eocene carbon isotope excursions in a lignite bearing succession at the southern edge of the proto-North Sea (Schöningen, Germany). Climate of the Past Discussions. https://doi.org/10.5194/cp-2021-81

Leon-Rodriguez, L., & Dickens, G. R. (2010). Constraints on ocean acidification associated with rapid and massive carbon injections: The early Paleogene record at ocean drilling program site 1215, equatorial Pacific Ocean. *Palaeogeography, Palaeoclimatology, Palaeoecology, 298*(3–4), 409–420.

Lomax, B. H., Lake, J. A., Leng, M. J., & Jardine, P. E. (2019). An experimental evaluation of the use of Δ13C as a proxy for palaeoatmospheric CO_2. *Geochimica et Cosmochimica Acta, 247*, 162–174.

Lourens, L. J., Sluijs, A., Croon, D., Zachos, J. C., Thomas, E., Röhl, U., Bowles, J., & Raffi, I. (2005). Astronomical pacing of late Palaeocene to early Eocene global warming events. *Nature, 453*, 1083–1087. https://doi.org/10.1038/nature03814

Mathews, R. P., Singh, B. D., Singh, H., Singh, V. P., & Singh, A. (2018). Characterization of Panandhro Lignite deposits (Kachchh Basin), western India: Results from the bulk geochemical and palynofloral compositions. *Journal of the Geological Society of India, 91*(3), 281–289.

McClure, K. J., & Lockwood, R. (2015). Relationships among Venericardia (Bivalvia: Carditidae) on the US Coastal Plain during the Paleogene. *Journal of Paleontology, 89*(3), 522–531.

McInerney, F. A., & Wing, S. L. (2011). The Paleocene–Eocene thermal maximum: A perturbation of carbon cycle, climate, and biosphere with implications for the future. *Annual Review of Earth and Planetary Sciences, 39*, 489–516. https://doi.org/10.1146/annurev-earth-040610-133431

Miller, K. G., Browning, J. V., Schmelz, W. J., Kopp, R. E., Mountain, G. S., & Wright, J. D. (2020). Cenozoic sea-level and cryospheric evolution from deep-sea geochemical and continental margin records. *Science Advances, 6*(20), eaaz1346.

Miller, K. G., Kominz, M. A., Browning, J. V., Wright, J. D., Mountain, G. S., Katz, M. E., Sugarman, P. J., Cramer, B. S., Christie-Blick, N., & Pekar, S. F. (2005). The Phanerozoic record of global sea-level change. *Science, 310*(5752), 1293–1298.

Miller, K. G., Mountain, G. S., Wright, J. D. & Browning, J. V. (2011). A 180-million-year record of sea level and ice volume variations from continental margin and deep-sea isotopic records. *Oceanography*, *24*(2), 40–53.

Mochales, T., Barnolas, A., Pueyo, E. L., Serra-Kiel, J., Casas, A. M., Samsó, J. M., Ramajo, J., & Sanjuán, J. (2012). Chronostratigraphy of the Boltaña anticline and the Ainsa Basin (southern Pyrenees). *Bulletin, 124*(7–8), 1229–1250.

Moussavou, B. M. (2015). Bivalves (Mollusca) from the Coniacian-Santonian Anguille Formation from Cap Esterias, northern Gabon, with notes on paleoecology and paleobiogeography. *Geodiversitas, 37*(3), 315–324.

Patriat, P., & Achache, J. (1984). India-Eurasia collision chronology has implications for crustal shortening and driving mechanism of plates. *Nature, 311*(5987), 615–621.

Paul, S., Sharma, J., Singh, B. D., Saraswati, P. K., & Dutta, S. (2015). Early Eocene equatorial vegetation and depositional environment: Biomarker and palynological evidences from a lignite-bearing sequence of Cambay Basin, western India. *International Journal of Coal Geology, 149*, 77–92.

Pérez, D. E. (2019). Phylogenetic relationships of the family Carditidae (Bivalvia: Archiheterodonta). *Journal of Systematic Palaeontology, 17*(16), 1359–1395.

Pietsch, C., Harrison, H. C., & Allmon, W. D. (2016). Whence the Gosport Sand (upper middle Eocene, Alabama)? The origin of glauconitic shell beds in the Paleogene of the U.S. Gulf Coastal Plian. *Journal of Sedimentary Research, 86*, 1249–1268. https://doi.org/10.2110/jsr.2016.72

Pujalte, V., Schmitz, B., & Baceta, J. I. (2014). Sea-level changes across the Paleocene–Eocene interval in the Spanish Pyrenees, and their possible relationship with North Atlantic magmatism. *Palaeogeography, Palaeoclimatology, Palaeoecology, 393*, 45–60.

Punekar, J., & Saraswati, P. K. (2010). Age of the Vastan Lignite in context of some oldest Cenozoic fossil mammals from India. *Journal of the Geological Society of India, 76*(1), 63–68.

Rana, R. S., Aug, M., Folie, A., Rose, K. D., Kumar, K., Singh, L., Sahni, A., & Smith, T. (2013). High diversity of acrodontan lizards in the Early Eocene Vastan Lignite Mine of India. *Geologica Belgica, 16*, 290–301.

Rao, M. R., Sahni, A., Rana, R. S., & Verma, P. (2013). Palynostratigraphy and depositional environment of Vastan lignite mine (Early Eocene), Gujarat, western India. *Journal of Earth System Science, 122*(2), 289–307.

Rose, K. D., Rana, R. S., Sahni, A., Kumar, K., Singh, L., & Smith, T. (2009). First tillodont from India: Additional evidence for an early Eocene faunal connection between Europe and India? *Acta Palaeontologica Polonica, 54*(2), 351–355.

Roy, P., & Mukherjee, P. (2017). Corbulid (Bivalvia) species from the Paleogene Mangrol Lignite Mine of Surat, Gujarat. *Journal Geological Society of India, 89*, 315–320.

Rust, J., Singh, H., Rana, R. S., McCann, T., Singh, L., Anderson, K., Sarkar, N., Nascimbene, P. C., Stebner, F., Thomas, J. C., & Kraemer, M. S. (2010). Biogeographic and evolutionary implications of a diverse paleobiota in amber from the early Eocene of India. *Proceedings of the National Academy of Sciences, 107*(43), 18360–18365.

Sahay, V. K. (2011). The hydrocarbon potential, thermal maturity, sequence stratigraphic setting and depositional palaeoenvironment of carbonaceous shale and lignite successions of Panandhro, northwestern Kutch Basin, Gujarat, Western India. *Central European Journal of Geosciences, 3*, 12–28.

Samanta, A., Bera, M. K., Ghosh, R., Bera, S., Filley, T., Pande, K., Rathore, S. S., Rai, J., & Sarkar, A. (2013). Do the large carbon isotopic excursions in terrestrial organic matter across Paleocene–Eocene boundary in India indicate intensification of tropical precipitation? *Palaeogeography, Palaeoclimatology, Palaeoecology, 387*, 91–103.

Samanta, A., Bera, M. K., & Sarkar, A. (2016). Climate-modulated sequence development in a tropical rift basin during the Late Palaeocene to Early Eocene super greenhouse Earth. *Sedimentology, 63*(4), 917–939.

Saraswati, P. K., Khanolkar, S., & Banerjee, S. (2018). Paleogene stratigraphy of Kutch, India: An update about progress in foraminiferal biostratigraphy. *Geodinamica Acta, 30*(1), 100–118.

Saraswati, P. K., Khanolkar, S., Raju, D. S. N., & Banerjee, S. (2016). An updated Eocene stratigraphy of Kutch. *Special Publication of the Geological Society of India, 6*, 25–31.

Saraswati, P. K., Sarkar, U., & Banerjee, S. (2012). Nummulites solitarius—Nummulites burdigalensis lineage in Kutch with remarks on the age of Naredi Formation. *Journal of the Geological Society of India, 79*(5), 476–482.

Schubert, B. A., & Jahren, A. H. (2012). The effect of atmospheric CO_2 concentration on carbon isotope fractionation in C3 land plants. *Geochimica et Cosmochimica Acta, 96*, 29–43.

Schubert, B. A., & Jahren, A. H. (2013). Reconciliation of marine and terrestrial carbon isotope excursions based on changing atmospheric CO_2 levels. *Nature Communications, 4*(1), 1–6.

Schulte, P., Scheibner, C., & Speijer, R. P. (2011). Fluvial discharge and sea-level changes controlling black shale deposition during the Paleocene–Eocene thermal maximum in the Dababiya Quarry section, Egypt. *Chemical Geology, 285*(1–4), 167–183.

Scotese, C. R. (2016). Tutorial: PALEOMAP paleo Atlas for GPlates and the paleoData plotter program. http://www.earthbyte.org/paleomap-paleo atlas-for-gplates/

Secord, R., Gingerich, P. D., Lohmann, K. C., & MacLeod, K. G. (2010). Continental warming preceding the Palaeocene–Eocene thermal maximum. *Nature, 467*(7318), 955–958.

Serra-Kiel, J., Hottinger, L., Caus, E., Drobne, K., Ferrandez, C., Jauhri, A. K., Less, G., Pavlovec, R., Pignatti, J., Samso, J. M., & Schaub, H. (1998). Larger foraminiferal biostratigraphy of the Tethyan Paleocene and Eocene. *Bulletin de la Société Géologique de France, 169*(2), 281–299.

Shukla, A., Singh, H., & Mehrotra, R. C. (2019). Fossil Wood of Subfamily Detarioideae (family Fabaceae) from the Paleogene of the Indian Subcontinent: Origin and Palaeo-dispersal Pathways. *Journal of the Geological Society of India, 94*(4), 411–415.

Singh, H. (2021). Palaeoenvironmental and taphonomic biases in palynological assemblages preserved in amber versus sediments from the Umarsar Lignite, Kutch Basin, Gujarat, India. *Historical Biology, 33*(10), 2305–2315.

Singh, P. K., Singh, V. K., Singh, M. P., & Rajak, P. K. (2017). Understanding the paleomires of Eocene lignbites of Kachchh Basin, Gujarat (Western india): Petrological implications. *International Journal of Coal Science and Technology, 4*(2), 80–101. https://doi.org/10.1007/s40789-017-0165-2

Slotnick, B. S., Dickens, G. R., Nicolo, M. J., Hollis, C. J., Crampton, J. S., Zachos, J. C., & Sluijs, A. (2012). Large-amplitude variations in carbon cycling and terrestrial weathering during the latest Paleocene and earliest Eocene: The record at Mead Stream, New Zealand. *The Journal of Geology, 120*(5), 487–505.

Sluijs, A., Bijl, P. K., Schouten, S., Röhl, U., Reichart, G. J., & Brinkhuis, H. (2011). Southern ocean warming, sea level and hydrological change during the Paleocene–Eocene thermal maximum. *Climate of the Past, 7*(1), 47–61.

Sluijs, A., Brinkhuis, H., Crouch, E. M., John, C. M., Handley, L., Munsterman, D., Bohaty, S. M., Zachos, J. C., Reichart, G. J., Schouten, S., & Pancost, R. D. (2008). Eustatic variations during the Paleocene–Eocene greenhouse world. *Paleoceanography, 23*(4), 4216. https://doi.org/10.1029/2008P A001615

Sluijs, A., Brinkhuis, H., Schouten, S., Bohaty, S. M., John, C. M., Zachos, J. C., Reichart, G.-J., SinningheDamsté, J. S., Crouch, E. M., & Dickens, G. R. (2007). Environmental precursors to rapid light carbon injection at the Palaeocene/Eocene boundary. *Nature, 450*, 1218–1222. https://doi.org/10.1038/nature06400

Sluijs, A., Van Roij, L., Harrington, G. J., Schouten, S., Sessa, J. A., Levay, L. J., Reichart, G. J. & Slomp, C. P. (2014). Warming, euxinia and sea level rise during the Paleocene–Eocene Thermal Maximum on the Gulf Coastal Plain: implications for ocean oxygenation and nutrient cycling. *Climate of the Past, 10*(4), 1421–1439.

Smith, A. G., Smith, D. G., & Funnel, D. M. (1994). *Atlas of Mesozoic and Cenozoic coastlines*. Cambridge University Press.

Speijer, R. P., & Morsi, A. M. M. (2002). Ostracode turnover and sea-level changes associated with the Paleocene–Eocene thermal maximum. *Geology, 30*(1), 23–26.

Stanley, S. M. (1972). Functional morphology and evolution of byssally attached bivalve mollusks. *Journal of Paleontology, 46*, 165–212.

Stassen, P., Thomas, E., & Speijer, R. P. (2012). Integrated stratigraphy of the Paleocene–Eocene thermal maximum in the New Jersey Coastal Plain: Toward understanding the effects of global warming in a shelf environment. *Paleoceanography, 27*(4), PA4210. https://doi.org/10.1029/2012P A002323

Storme, J. Y., Dupuis, C., Schnyder, J., Quesnel, F., Garel, S., Iakovleva, A. I., Iacumin, P., Di Matteo, A., Sebilo, M., & Yans, J. (2012). Cycles of humid-dry climate conditions around the P/E boundary: New stable isotope data from terrestrial organic matter in Vasterival section (NW France). *Terra Nova, 24*(2), 114–122.

Velde, B. (2014). Green clay minerals. In H. D. Holland & K. K. Turekian (Eds.), *Treatise on geochemistry* (2nd ed., Vol. 9, pp. 351–364). Elsevier.

Wang, G., Jia, Y., & Li, W. (2015). Effects of environmental and biotic factors on carbon isotopic fractionation during decomposition of soil organic matter. *Scientific Reports, 5*(1), 1–11. https://doi.org/10.1038/srep11043

Westerhold, T., Röhl, U., Donner, B., & Zachos, J. C. (2018). Global extent of early Eocene hyperthermal events: A new Pacific benthic foraminiferal isotope record from Shatsky Rise (ODP Site 1209). *Paleoceanography and Paleoclimatology, 33*(6), 626–642.

Westerhold, T., Röhl, U., Laskar, J., Raffi, I., Bowles, J., Lourens, L. J., & Zachos, J. C. (2007). On the duration of magnetochrons C24r and C25n and the timing of early Eocene global warming events: Implications from the Ocean Drilling Program Leg 208 Walvis Ridge depth transect. *Paleoceanography, 22*(2), PA2201.

Willard, D. A., Donders, T. H., Reichgelt, T., Greenwood, D. R., Sangiorgi, F., Peterse, F., Nierop, K. G., Frieling, J., Schouten, S., & Sluijs, A. (2019). Arctic vegetation, temperature, and hydrology during Early Eocene transient global warming events. *Global and Planetary Change, 178*, 139–152.

Wright, J. D. (2001). Cenozoic climate—Oxygen isotope evidence. In J. Steele, S. Thorpe, & K. Turekian (Eds.), *Encyclopedia of ocean sciences* (pp. 415–426). Academic Press.

Zamagni, J., Mutti, M., Ballato, P., & Košir, A. (2012). The Paleocene–Eocene thermal maximum (PETM) in shallow-marine successions of the Adriatic carbonate platform (SW Slovenia). *Bulletin, 124*(7–8), 1071–1086.

Publisher's Note